https://doi.org/10.5194/egusphere-2025-5506
Preprint. Discussion started: 23 December 2025

Reaction-transport modelling of methane cycling beneath the Greenland Ice Sheet

Philip Píka[1,2], Sandra Arndt[2], Petra Klímová[1], Guillaume Lamarche-Gagnon[3], Marek Stibal[1]

1: Department of Ecology, Faculty of Science, Charles University, Prague, Czech Republic. 2: Université libre de Bruxelles, Brussels, Belgium. 3: Centre for ice, Cryosphere, Carbon and Climate (iC3), Department of Geosciences, UiT The Arctic University of Norway, 9037 Tromsø, Norway.

Correspondence: Philip Píka (pikap@natur.cuni.cz)

1 Abstract

Glacial and ice sheet advances have buried large amounts of organic matter (OM), which under anoxic subglacial conditions can be microbially converted into methane (CH_4). Although CH_4 emissions have been observed at glacier margins, the capacity of subglacial environments to sustain such fluxes remains uncertain. To address this, we developed a reaction–transport model (RTM) to simulate CH_4 production, transformation, and transport in sediments beneath warm-based regions of the Greenland Ice Sheet (GrIS) margin. The model explores a wide range of environmental conditions, including sediment thickness, OM quantity and reactivity, O_2 availability, and methanotrophic activity.

Model simulations show that subglacial sediments are largely anoxic. Oxygen (O_2) penetration into subglacial sediments is generally restricted to the upper few tens of centimetres, with an average penetration depth of 22.8 cm. Microbial OM degradation and aerobic CH_4 oxidation (AeOM) represent the main O_2 sinks. Their relative contributions vary with CH_4 availability. AeOM dominates in methane-rich sediments, whereas OM degradation prevails in methane-poor environments. Modelled depth-integrated methanogenesis rates range from 0.1 to 1600 mmol-CH_4 m^{-2} yr^{-1} (mean 73 mmol-CH_4 m^{-2} yr^{-1}) and are primarily controlled by OM reactivity, with sediment depth and OM concentration exerting only a small secondary influence. This sensitivity of CH_4 production rates to OM reactivity can produce sharp thresholds, where small decreases in reactivity strongly suppress CH_4 fluxes. A highly variable fraction of the generated CH_4 is consumed by AeOM within the shallow oxygenated zone, and is controlled by OM reactivity and the AeOM rate constant. Resulting net diffusive CH_4 fluxes can range between 0-234.7 mmol m^{-2} yr^{-1}. Results show that even shallow sediments (<1 m) can sustain a significant CH_4 release into the subglacial environment when highly reactive OM is available, while oxidation efficiency tends to decline in thick, OM-rich deposits.

https://doi.org/10.5194/egusphere-2025-5506
Preprint. Discussion started: 23 December 2025

Comparison with field measurements of CH_4 export data from southwest GrIS catchments suggests that observed fluxes could be already sustained by subglacial sediments that contain as little as 0.6 wt% of relatively unreactive OM assuming a catchment sediment cover of 10 % with sediment depths of 9 m.

2 Introduction

Fluctuations in glacier extent during past glacial periods repeatedly reshaped high-latitude landscapes by overriding tundra, boreal forest, and peatland ecosystems, burying vast stocks of organic matter (OM) (Weitemeyer and Buffett, 2006; Wadham et al., 2008). Beneath the Greenland Ice Sheet (GrIS), these stocks are estimated to contain 0.5 - 27 Pg of carbon (Wadham et al., 2019). Once isolated beneath the ice, microbial respiration of OM consumes residual oxygen (O_2) and other terminal electron acceptors (TEAs) (Bottrell and Tranter, 2002; Tranter et al., 2005), creating anoxic conditions conducive to methanogenesis, the microbial production of the potent greenhouse gas methane (CH_4) (Wadham et al., 2008, 2012; Stibal et al., 2012). This CH_4 may then accumulate in subglacial sediments as immobile gas hydrates, in the presence of a gas-hydrate stability zone (Wadham et al., 2012; Lamarche-Gagnon et al., 2019), or as free gas that dissolves in porewater. Dissolved CH_4 diffuses into oxidizing sediment layers and, upon entering the subglacial hydrological system (Michaud et al., 2017), can be transported laterally and ultimately released into the atmosphere. The presence of CH_4-oxidizing clades found within microbial assemblages of glacial outlets (Lamarche-Gagnon et al., 2019; Vrbická et al., 2022; Znamínko et al., 2023; Hatton et al., in review, 2025) coupled with direct evidence for active CH_4 oxidation (Dieser et al., 2014; Strock et al., 2024), suggests that these environments may host an internal biological sink that could mitigate the net export of CH_4 from the subglacial environment (Dieser et al., 2014; Michaud et al., 2017).

While field observations confirm that CH_4 is being released from melting glacier and ice sheet margins (Stibal et al., 2012; Dieser et al., 2014; Christiansen and Jørgensen, 2018; Lamarche-Gagnon et al., 2019; Sapper et al., 2023; Hatton et al., in review, 2025), the capacity of these systems to sustain such fluxes remains a critical unknown, mostly due to limited understanding of the physico-chemical conditions within the subglacial environment. Primary among these uncertainties is the nature of the buried OM, specifically its origin (Bierman et al., 2014; Blard et al., 2023), reactivity and age (Kohler et al., 2017; Vinšová et al., 2022), and concentration (Yde et al., 2010; Stibal et al., 2012; Bhatia et al., 2013a), and its spatial distribution under the ice (Maier et al., 2021). Furthermore, the lack of direct measurements of the prevailing redox conditions that govern microbial activity severely limits our ability to assess the spatial variability of CH_4 production and oxidation potential in subglacial environments.

To address this knowledge gap, we utilize a reaction-transport model (RTM) to investigate biogeochemical processes in the GrIS subglacial ecosystem. We assess the potential for biogenic CH_4 production, consumption, and release from subglacial sediments underneath the warm-based margins of the GrIS. The model accounts for the key biogeochemical and physical processes, including microbial CH_4 production (methanogenesis) and CH_4 oxidation, and diffusive transport in and from subglacial sediments. We conduct a sensitivity study with the RTM over a large ensemble of scenarios to explore a wide range

https://doi.org/10.5194/egusphere-2025-5506
Preprint. Discussion started: 23 December 2025

of plausible environmental conditions. These scenarios vary key parameters, including subglacial sediment thickness, OM concentration and reactivity, O_2 concentration, and methanotrophic activity, all of which are constrained by observations from subglacial and other similar environments. We present a case study of two well-studied catchments in SW Greenland where we calculate lateral fluxes and estimate in-stream CH_4 loss. Finally, we discuss model results in the context of available field observations of CH_4 dissolved in meltwater, thus assessing the potential contribution of subglacial CH_4 to regional carbon budgets and cryosphere-climate feedback.

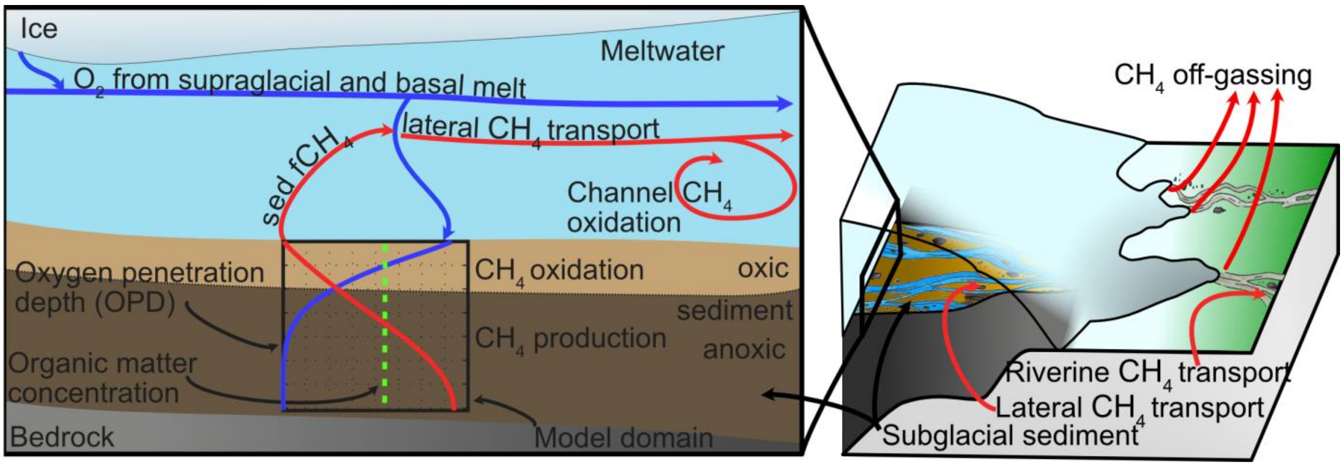

Figure 1: Conceptual diagram of subglacial and proglacial forefield transport and biogeochemical processes influencing CH_4 sources and sinks. Arrows indicate flux directions. The left panel highlights subglacial sediments and hydrological controls on CH_4 dynamics; the right panel shows an overview of subglacial and proglacial zone processes. The sediment biogeochemical model (BRNS) used in this study is outlined in black (left panel). Terminology here is consistent with that used throughout the text. Subglacial sediment CH_4 flux (sed. fCH_4) is calculated as $F_{CH_4,sed} = \int R_{Mgen} - \int R_{MOx}$ and glacial outlet flux as $F_{CH_4,outlet} = F_{CH_4,sed} \cdot A_{catchment} \cdot (1 - k_{ox} \cdot T_{transit})$.

3 Methods

3.1 BRNS - a reaction-transport network

We use a one-dimensional reaction-transport model (RTM), the Biogeochemical Reaction Network Simulator (BRNS, Regnier et al., 2002) and adapt it to subglacial sedimentary environments. BRNS is an adaptive simulation environment, suitable for large, mixed kinetic-equilibrium reaction networks, and has been successfully adopted across a wide range of sedimentary environments (Dale et al., 2008; Thullner, Dale and Regnier, 2009; Puglini et al., 2019). It accounts for methanogenesis, aerobic CH_4 oxidation (AeOM) and for advective and diffusive CH_4 transport to quantitatively assess the potential for biogenic CH_4 production and export from subglacial sediments underneath the GrIS for a wide range of plausible environmental conditions. Below, we describe how the model is set up to simulate subglacial soft sediments and the assumed boundary conditions.

https://doi.org/10.5194/egusphere-2025-5506
Preprint. Discussion started: 23 December 2025

The model solves the set of coupled one-dimensional conservation equations in porous media given by

$$\frac{\partial \sigma C_i}{\partial t} = D_i^* \sigma \frac{\partial^2 C_i}{\partial z^2} + \alpha_i \sigma (C_{i,0} - C_i) + \sigma \sum_j s_i^j R^j$$

where, the first and second terms describe the diffusive and advective transport, respectively, where C_i represents the concentration of species i, t denotes time, and z is the sediment depth. For solid species the porosity term is given by $\sigma = (1 - \phi)$, whereas for dissolved species porosity assumes $\sigma = \phi$. The effective molecular diffusion coefficient of dissolved species i is given by D_i^* ($D_i = 0$ for solid species). The third term, $\Sigma_j s_i^j R^j$ denotes the sum of consumption/production processes, where the stoichiometric coefficient of species i is given by s_i^j for the kinetically controlled reaction j, with rate R^j. The implemented reaction network (Table C1) considers the most important primary and secondary redox reactions, equilibrium reactions, mineral dissolution and precipitation, and adsorption and desorption processes affecting the dissolved and solid species that are explicitly resolved in the model.

Here, we explicitly simulate the coupled, steady-state reaction/transport dynamics of OM, O_2, and CH_4 in GrIS marginal subglacial sediments. We assume that modelled diffusive transport in the liquid or gas phase is the dominant transport process in subglacial sediment environments. We assume negligible advective transport of solids and solutes across either the top (ice) or bottom (bedrock) layer. Top layer sediment mixing (cryoturbation) is also assumed to be negligible throughout the sediment column.

The following section provides a short overview of the description of OM, O_2, and CH_4 dynamics implemented in the model. Table C2 summarizes the range of parameter values and boundary conditions used in the model.

3.2 Transport model

Our transport model assumes diffusive transport is the only dominant transport process in subglacial sediment environments. Molecular diffusion term is described by

$$F|_{diff} = D_i^*(T,S) \cdot \sigma(z) \cdot \frac{\partial C_i}{\partial z}$$

The effective diffusion coefficient, D_i^*, is given by:

$$D_i^*(T,S) = \frac{D_i(T,S)}{1 - ln(\phi^2)}$$

where D_i(T,S) is the species-dependent molecular diffusion coefficient corrected for in-situ temperature (T, in °C), salinity (S, in PSU) and tortuosity ($\Phi = 1 - ln(\phi^2)$) (Boudreau, 1997). D_i(T,S) is linearly interpolated for the in-situ temperature, T (in °C), using a zero-salinity and zero-degree diffusion coefficient, D_i^0 (T = 0,S = 0) and a temperature-dependent diffusion coefficient D_i^T (Soetaert, Herman and Middelburg, 1996).

$$D_i(T,S) = D_i^0(T = 0, S = 0) + D_i^T \cdot T$$

Sediment porosity (Φ) starts at 0.5 and decreases exponentially across the model domain until it reaches 0.25, a range and depth evolution consistent with values reported in (Dow et al., 2013; Lamarche-Gagnon et al., 2019). Similar ranges are found in measurements from western Antarctica (0.4 - 0.5) (Bougamont, Tulaczyk and Joughin, 2003; Kulessa, Hubbard and Brown, 2006).

3.3 Biogeochemical Reaction Network

3.3.1 Primary redox reactions

Primary redox reactions considered in the reaction network include the OM degradation pathways (see list of the reaction network in Table C1): aerobic respiration (r1) and methanogenesis (r2). The degradation rate of each pathway depends on the concentration of the TEAs and is kinetically limited by the presence of more powerful TEAs, reflecting their sequential utilization in the order of their decreasing yield in Gibbs energy from its half-reaction. Once the TEAs are consumed, the remaining OM is degraded via methanogenesis as the final step.

While this study prioritizes aerobic respiration and methanogenesis as the primary redox pathways, the subglacial environment contains several other TEAs whose inclusion in reactive transport models presents significant challenges. Many TEAs that are energetically more favorable than methanogenesis (such as SO_4^{2-}, NO_3^-, and bioavailable Fe(III)) have been measured in meltwaters (Tranter et al., 2002; Statham, Skidmore and Tranter, 2008; Bhatia et al., 2013; Hawkings et al., 2014, 2018) and their role in reflecting anoxic biogeochemical processes in the subglacial environment is well-documented (Tranter et al., 2002). Extrapolating discharge-weighted TEA concentrations to (dissolved and/or solid) concentrations within subglacial sediment suitable for RTM inputs is highly uncertain. This would introduce model parameters that are difficult to constrain, making the model unnecessarily complex and difficult to verify its results, since in-situ measurements of sediment composition are scarce as they are challenging to sample. Studies have observed both the rapid consumption of nitrate by denitrifying bacteria in basal ice sediment (Yde et al., 2010) and elevated bioavailable iron (Fe(III) and Fe(II)) concentrations in meltwater (Bhatia et al., 2013; Hawkings et al., 2014), highlighting their role in OM degradation via iron reduction. However, translating these findings into applicable boundary conditions is not as straightforward, and additionally the contribution of some processes, like iron reduction, may be minor despite the high TEA concentration (Lenstra et al., 2023). Therefore, given the significant uncertainties in constraining the parameters for these processes, we simplify this reaction network to focus primarily on aerobic respiration and methanogenesis.

Findings from subglacial sediment at the glacier margin indicate CH_4 originates from both acetoclastic methanogenesis (Lamarche-Gagnon et al., 2019; Pain et al., 2021; Christiansen et al., 2021; Hatton et al., in review, 2025) and hydrogenotrophic CH_4 production (Stibal et al., 2012; Telling et al., 2015). Their relative importance under varying environmental conditions, such as substrate availability, carbon oxidation state, pH, temperature, or redox potential in subglacial sediments, is yet to be determined. We thus aggregate methanogenic pathways into a single terminal reaction: OM $\rightarrow CH_4 + CO_2$. The $CH_4:CO_2$ ratio of 1 assumes an OM oxidation state of 0 (Burdige et al., 2016), and is usually applicable under optimal methanogenic

https://doi.org/10.5194/egusphere-2025-5506
Preprint. Discussion started: 23 December 2025

conditions (Symons and Buswell, 1933; Nilsson and Öuist, 2013), which are unlikely to be found in subglacial sediments. Nevertheless, this bulk approach, common in models of soils, sediments, and aquatic systems (Thullner et al., 2009; Regnier et al., 2011; Burdige et al., 2016; Puglini et al., 2019), avoids tracking intermediates like acetate or H_2, which would require constraining additional poorly constrained parameters, thereby introducing additional uncertainty. Since methanogens ferment only products from OM degradation, we assume their activity scales with overall OM degradation (k × [OM]). This simplification efficiently captures observed CH_4 dynamics without compromising model performance.

The OM degradation rate, R_{OM}, within the sediment column is described by a reactive continuum model (RCM, see Boudreau and Ruddick, 1991). The RCM assumes a continuous and dynamic distribution of OM fractions over a range of reactivities and encapsulates the decrease in apparent reactivity with depth (and thus age) as the most reactive fractions are successively degraded. R_{OM} is given by:

$$R_{OM} = -\int_0^{\infty} k \cdot om(k,t)dk$$

where $om(k,t)$ denotes a probability density function that determines the concentration of OM having a degradability between k and k + dk at time t, with k being analogous to a first-order rate constant. The initial distribution of organic fractions, $om(k,t=0)$, may take different mathematical forms and cannot be inferred by observations. It is given by:

$$om(k,t=0) = \frac{OM(0) \cdot a^{\nu} \cdot k^{\nu-1} \cdot e^{-a \cdot k}}{\Gamma(\nu)}$$

where OM(0) is the initial OM concentration, $\Gamma(\nu)$ is the gamma function, a is the average lifetime of the more reactive fractions of the spectrum of the OM mixture, while ν is a dimensionless scaling parameter shifting the Gamma distribution near k = 0 towards a more or less reactive OM mixture. The two free, positive parameters a and ν completely describe the type of OM mixture over the range of k-values and therefore, the overall OM reactivity. High ν and low a values indicate a mixture of OM dominated by more readily degraded OM fractions, i.e. a higher reactivity. On the other hand, low ν and high a values, indicate a larger contribution of less reactive compounds to the total OM pool, i.e. a lower reactivity.

Under these assumptions, the decrease of bulk OM concentration as a function of depth, OM(z), is given by:

$$OM(z) = OM(0) \cdot k(a,\nu) = OM(0) \cdot (\frac{a}{a + age(z)})^{\nu}$$

where age(z) denotes the age of the sediment layer at depth z (see sec. 3.6.2 and sec. 3.6.3).

3.3.2 Secondary redox reactions

The upward migration of biologically produced reduced species (e.g. NH_4^+ and CH_4), into more oxidizing sediment layers leads to their re-oxidation via a set of secondary redox reactions, which sustain a continuous recycling of these redox sensitive elements. Specifically, we focus only on aerobic CH_4 oxidation (AeOM, see table C1) as top layers in sediments are likely oxic and acting as a CH_4 sink. The bimolecular rate laws of secondary redox reactions are based on (Wang and Van Cappellen, 1996).

https://doi.org/10.5194/egusphere-2025-5506
Preprint. Discussion started: 23 December 2025

CH_4 is either consumed aerobically or anaerobically (i.e., in the absence of O_2). The former is relevant in oxic and sulfate-poor freshwater sediments, such as wetlands, lakes, or soils (Knoblauch et al., 2008; Oh et al., 2020), while the latter requires an absence of O_2 and the presence of TEAs such as sulfate or ferric iron, which are common in marine sediments (Egger et al., 2018), and in sub-Arctic lake sediments (Martinez-Cruz et al., 2017). The O_2 supply derives from a combination of surface and basal melt and is more important beneath the ablation zone of the ice sheet (see sec. 4.1), where large volumes of O_2-rich surface water reach the subglacial bed through moulins and crevasses, where they subsequently fuel biogeochemical redox reactions. The importance of AeOM relative to anoxic oxidation pathways is supported by an analysis of subglacial meltwater in SW Greenland using clumped CH_4 isotopes (Adnew et al., 2025). The likely minor role of AOM is also supported by the relatively low sulfate concentrations, as reported for subglacial porewater by others (6-26 µM; although values up to 244 µM have also been reported, Christ et al., 2021; Lawson, 2012; Graly et al., 2014), and a recent subglacial sediment core porewater sample collection (~1.7-4 µM SO_4^{2-}) under Isunnguata Sermia, SW GrIS (Klímová, Stibal et al., unpublished data). Additionally, unpublished incubation experiments with basal sediments using commonly available TEA (SO_4^{2-}, Fe(III) and Mn(IV)) supported the assumption that AOM was negligible (Klímová, Stibal et al., in preparation, 2025). Consequently, in this study, we focused on AeOM rather than AOM, as the primary biological CH_4 sink. We formulate AeOM by aerobic methanotrophs according to the bimolecular reaction equation:

$$CH_4 + 2O_2 \rightarrow CO_2 + 2H_2O$$

and its rate law is given by

$$rAeOM = kAeOM[CH_4][O_2]$$

where the rate constant for AeOM, k_{AeOM}, is further examined as a model parameter in our sensitivity analysis, since it influences the oxidation efficiency of aerobic methanotrophs.

This equation assumes kinetic and thermodynamic factors, and biomass dynamics are implicitly accounted for in the rate constant (Dale et al., 2006; Regnier et al., 2011). The range for k_{AeOM} is discussed below (sec. 3.6.6).

3.4 Boundary conditions

Dirichlet conditions (fixed concentrations) $c_i(z=0) = c_{i,0}$ are imposed for dissolved species at the upper boundary (top of the sediment model domain), while for solid species Robin type (constant flux) conditions are set: $J_s = \rho \cdot (1-\phi) \cdot (v \cdot c_i - D_{bio}\frac{\partial c_s}{\partial z})_{z=0}$, where c_s indicates the concentration of a solid species, ρ is the sediment density (2.0 g cm^{-3}) and ϕ is the sediment porosity. At the lower boundary of the model domain, a no-flux ($\frac{\delta c_i}{\delta z} = 0$, Neumann condition) is applied for all species, which implies a negligible influence of biogeochemical processes in sediments underlying the model domain (Boudreau, 1997), i.e. no thermogenic CH_4 diffusing upward through rock cracks.

https://doi.org/10.5194/egusphere-2025-5506
Preprint. Discussion started: 23 December 2025

3.5 Numerical solution

The transport term for dissolved species is discretized using the Crank-Nicolson algorithm (Regnier et al., 1997). The reaction terms are solved simultaneously by solving the Jacobian Matrix. Transport and reaction terms are solved sequentially in each time step. The sediment model domain is subdivided into an irregular grid composed of 173 to 579 nodes with increasing grid resolution from 0.05 cm to 1.25 cm, then to 5.0 cm until z_{max}. This avoids numerical instabilities that may emerge due to the succession of strong concentration gradients created by the fast secondary redox reactions in the upper part of the sediment column. The transient model simulations are run until steady-state is reached using an adaptable time step allowing sufficient numerical precision if needed, but still permitting considerable speed-up in computation time.

3.6 Setup of the Environmental Model ensemble

To identify the main controls on the depths of the methanogenic zone in subglacial sediments (i.e. z > O_2 penetration depth, OPD), as well as CH_4 flux from subglacial sediments, we ran a model ensemble (n = 210) over the below defined plausible range of subglacial environmental conditions. To this end, we used the Latin hypercube sampling approach to select 210 input vectors $\chi^j(j = 1, \ldots, r)$ each with variations in the model parameters i (i.e., sediment thickness, subglacial OM concentration and reactivity, dissolved O_2 and aerobic methanotrophic activity), as suggested in the Sensitivity Analysis for Everyone (SAFE) MATLAB toolbox (Pianosi, Sarrazin and Wagener, 2015). More on the sensitivity analysis below. The following sections provide an overview and rationale for the chosen parameter ranges, and a description of the sensitivity measures calculated.

3.6.1 Subglacial Sediment depth

The volume of soft subglacial sediment is critical for creating an environment suitable for microbial methanogenic activity and its subsequent upward diffusion towards the sediment-water interface and into the subglacial hydrological network. However, sparse data on both sediment thickness and spatial distribution hinder an accurate assessment. Nevertheless, a growing body of evidence from along the western margin of the GrIS suggests the ice sheet bed is characterized by a mix of hard bedrock with only thin coarse sediments (Harper et al., 2017) and layers of unfrozen till/soft sediment (Booth et al., 2012; Dow et al., 2013; Kulessa et al., 2017; Ruskeeniemi et al., 2018) of up to several tens of meters in thickness (Walter et al.,, 2014). For instance, under the glacier tongue of Isunnguata Sermia (SW Greenland), an unfrozen till layer of maximum 10 m thickness was measured (Ruskeeniemi et al., 2018), while its neighboring Russell Glacier is also hypothesized to be underlain with soft sediment (Dow et al., 2013). In this study, we simulate the sediment depth down to 15 m and assume a spatial extent between 1 - 100% of the total catchment area.

https://doi.org/10.5194/egusphere-2025-5506
Preprint. Discussion started: 23 December 2025

3.6.2 Organic matter concentration and depth-profile

OM concentration is a key parameter influencing the subglacial biogeochemical processes. Several studies have reported bulk OM concentrations in subglacial sediments under the GrIS, yet only a few focus on thawed-bed areas of glaciers, where unfrozen till under the marginal ablation zones of the GrIS is assumed to be biologically active. The reported range from basal ice at glacier margins is 0.01 - 1.52 wt%, with a mean value of 0.21 wt% (Yde et al., 2010; Stibal et al., 2012; Graly, Drever and Humphrey, 2017). A recent pan-Arctic review of marginal subglacial OM (~0.5 wt%, Vinšová et al., 2022) corroborates these low concentrations found previously. We are aware that higher values of OM concentration up to 1.7 wt% at GISP2 (Bierman et al., 2014) and even 47.7 wt% at Camp Century (Christ et al., 2021) have been reported; however, these sediments were collected frozen from a cold-based part of the GrIS, suggesting good preservation of frozen OM and are not necessarily representative of marginal sediments underlying warm-bed glaciers, in which microbes play an active role in transforming OM (Christiansen et al., 2021; Vinšová et al., 2022).

We assume a constant OM concentration with subglacial sediment depth, due to the intense reworking of soils in proglacial areas during the glacier re-advance. Therefore, we prescribe the depth profile once as constant across the model domain. While this approach likely overestimates the depth-integrated OM content, which in turn affects all redox pathways, the current lack of OM concentration depth profiles in marginal subglacial sediment leaves too much room for speculation regarding the nature of a decreasing profile.

3.6.3 Organic matter reactivity

The RCM requires the parameters a and ν to fully describe the OM reactivity (i.e. its quality, or bioavailability); however, these are yet to be constrained for subglacial systems due to the scarcity of observational data. As revealed by plant fossils found in soil/sediment samples from several sites across Greenland (Dye 3, GRIP, John Evans Glacier, Camp Century; Willerslev et al., 2007) and in biomarker analysis of freshly thawed basal sediment (Vinšová et al., 2022), environments such as boreal forest and tundra dominated ice free areas in Greenland during the Holocene Climate Optimum. Linking paleo-vegetation analogues to present-day ecosystems is a first step to estimate the likely range in OM reactivities stored in subglacial sediments.

A recent effort to constrain the RCM parameter using incubation experiments of OM in high latitude soils (i.e., permafrost, boreal forest, and tundra vegetation), puts the range of parameter ν between 0.0012 and 1.7 with a median of 0.04; and a mean of 0.21, while parameter a is narrowed down to 0.0065 - 3.75 years; median 0.18; mean 0.9 years (Arndt, in review, 2025). Ranges are limited to their 5% and 95% quantiles respectively to prevent a skewed distribution due to outliers. The uncertainty in constraining the range in OM reactivity is further reduced by limiting parameter a to its mean value, instead of the full range, such that parameter ν solely determines the overall reactivity, k (see Eq. OM k). This simplification applies when parameter a is much lower (a_{max}= 14.6 yrs) than the age of the OM in subglacial sediments (age = 4000 yrs, see Eq. OM k). The mean age of the OM exported from the subglacial environment in the Kangerlussuaq sector of the SW GrIS range between

5000 - 9000 years depending on subglacial drainage system development (Kohler et al., 2017) and reflects a mix of Holocene and Eemian materials.

Fig. 2 a shows the temporal evolution of OM k as a function of parameter a, expressed as $k = f(a, \nu = const)$. Here, the selected scenarios illustrate plausible values for parameter a in high-latitude soils (a_{min} = 10^{-9} yrs; a_{max} = 14 yrs), yet also include a case with $a = 1000$ years to demonstrate how OM k stabilizes to a time-invariant value after a few hundred years (red line in Fig. 2 a). Thus, we chose the median value of 0.2 years for parameter a for our model setup. This simplification holds for the time scales considered relevant here (i.e. the Holocene) and would not be applicable for OM buried during the Eemian period. On the other hand, Fig. 2 b demonstrates the considerable influence of parameter ν on OM k, $k = f(a = const, \nu)$, for the range of values found in high latitudes (Arndt, in review, 2025). Higher values of ν indicate a greater proportion of reactive compounds in the initial OM mixture. We therefore varied ν across the entire range of plausible values, i.e. between 0.0012 and 0.9.

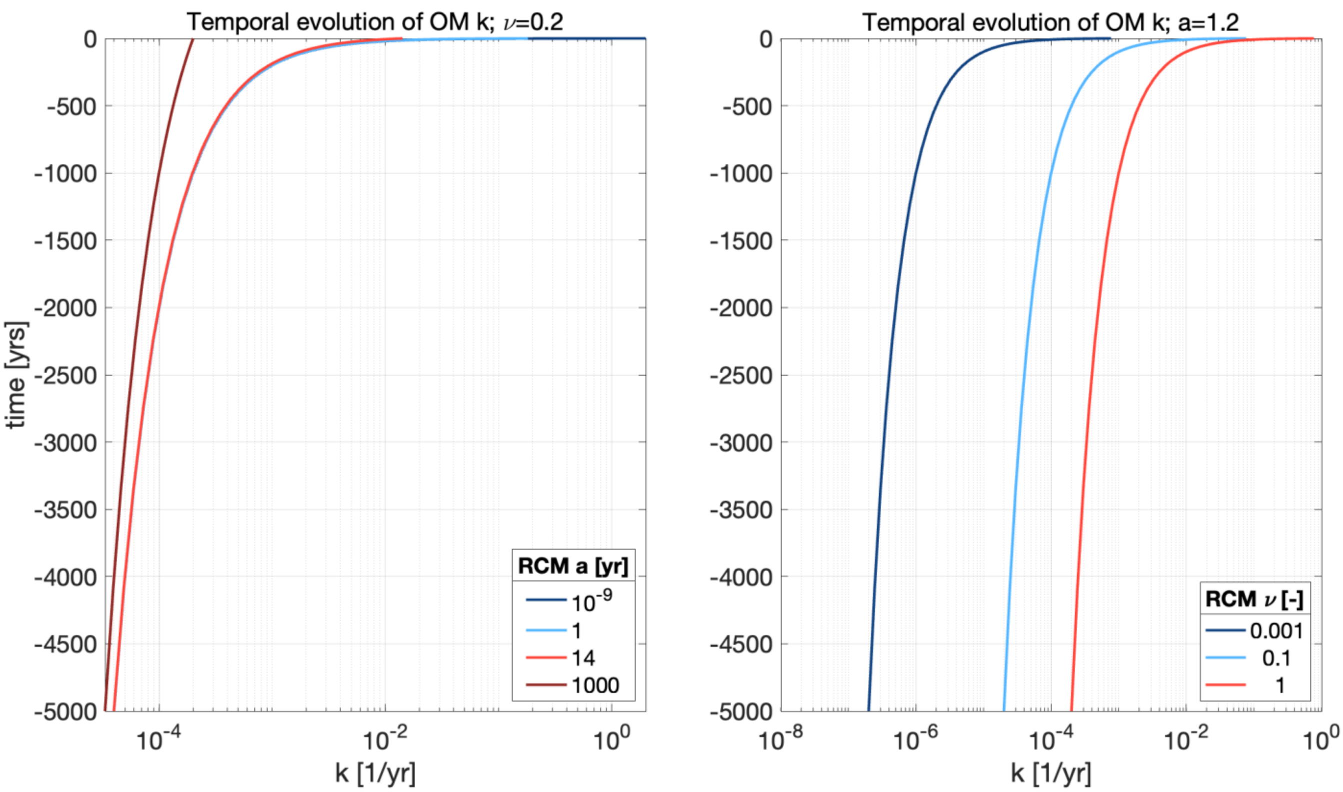

Figure 2: Change in organic matter reactivity (OM k) over time, modelled with the Reactive Continuum Model (RCM) using the equation k=ν/(a+t) from 5 kyr ago till present-day. Left panel: The effect of parameter a on OM reactivity. Parameter ν=0.2, while parameter a varies from 10^{-9} to 1000 years. OM k converges to similar values once the elapsed time (t or age) is much greater than a. The curve for a=1,000 years deviates significantly because the 5,000-year timescale is not long enough to satisfy the t≫a condition. Right panel: The effect of parameter ν on OM reactivity, when parameter a=1.2 years, while ν varies from 0.001 to 1. This panel

shows that an increase in parameter ν leads to an overall higher reactivity, as a larger ν implies a greater contribution of highly reactive compounds in the initial OM mixture.

3.6.4 Temperature

Temperature in the subglacial sediments is assumed stable throughout the year at -0.5 ˚C. This represents the mean of several temperature measurements of basal ice at the glacier margin and inland of the Isunnguata Sermia glacier (Harrington, Humphrey and Harper, 2015), and we assume these are reflective of the general thermal state of soft subglacial sediments. We ignore the influence of a geothermal heat gradient on the redox chemistry and assume a constant temperature throughout the sediment column, which, given the relatively shallow simulated sediments (0.2 - 15 m) is assumed reasonable, i.e. assuming a moderate geothermal heat flux of 56 mWm^{-2} would lead to less than 0.5 ˚C increase over simulated 15 m (Colgan et al., 2022).

3.6.5 Redox conditions in the subglacial drainage system

Redox conditions can vary within the drainage system, and there is evidence for both oxic and anoxic environments (Bottrell and Tranter, 2002; Tranter et al., 2002). The redox state of the subglacial environment depends on the supply of O_2 and its consumption rates within the seasonally developing drainage system. Underneath the GrIS, O_2 is supplied through supraglacial or basal meltwaters. Supraglacial meltwater saturated with O_2 enters the subglacial environment through moulins, increasing subglacial O_2 concentration and creating oxic conditions. In addition, basal melt also supplies O_2 trapped in air bubbles in the melting basal ice overlaying subglacial sediments. Assuming basal melt rates of 6.1 - 2.1 mm yr^{-1} (Dahl-Jensen et al., 2003; Buchardt and Dahl-Jensen, 2007; Harper et al., 2021) and O_2 concentrations of 291 - 446 µM in basal ice (gas bubble concentration from Herron, Hoar and Langway, 1979), this process could supply a baseline flux of 1.7 - 8.9 mmol m^{-2} yr^{-1}. The rates of O_2 consumption within the subglacial drainage system remain poorly constrained, but the presence of subglacial sediments likely increases local O_2 consumption due to microbial degradation of OM and oxidation of reduced species, such as CH_4.

The spatial extent of oxic environments under the ice and its temporal evolution over the melt season remain unassessed. Nevertheless, integrated water chemistry signals measured at the glacier margins strongly suggest that anoxic conditions prevail over large parts of the subglacial drainage system over prolonged periods of time (Bottrell and Tranter, 2002; Tranter et al., 2005). To fully cover the spectrum of plausible redox conditions at the sediment-water/ice interface, we here explore the full range of dissolved subglacial water O_2 (T= -0.5 ˚C, S=0 PSU) concentrations from anoxia (0 µM) to fully oxic conditions (456 µM). It is important to note that we neglect here seasonality in O_2 concentration, i.e. O_2 replenishing supraglacial meltwater, hence assuming a given redox state prevails over the entire simulation time. Potential caveats of this are discussed below.

https://doi.org/10.5194/egusphere-2025-5506
Preprint. Discussion started: 23 December 2025

3.6.6 Rate constant for aerobic CH_4 oxidation

Soil microbial processes, including AeOM, are regulated by microbial biomass and community composition, with additional control from environmental factors such as temperature, CH_4 availability, moisture, pH, and soil type (Murguia-Flores et al., 2018). The effects of these drivers on AeOM are poorly constrained and rarely represented explicitly in models. Instead, rate constants are calibrated against observations, thereby implicitly accounting for factors that are not explicitly described in the model formulation and tend to show a strong variability across different environments.

The rate constant for the AeOM (k_{AeOM}) is a key parameter that exerts significant control on AeOM and thus the estimated diffusive CH_4 flux. Previously published constants in Arctic soils vary between [2.7 - 3.4] × 10^9 cm^3 mol^{-1} yr^{-1} (Murguia-Flores et al., 2018), while in coastal marine sediments they span (9.4 - 150) × 10^7 cm^3 mol^{-1} yr^{-1} (Mao et al., 2022). In contrast, much higher constants have been used for shallow Arctic Ocean shelf sediments (10^{13} cm^3 mol^{-1} yr^{-1} ;Puglini et al., 2019). Here, we adopt a conservative approach to avoid speculation on the oxidation efficiency, limiting the range of range of published k_{AeOM} to [10^6 - 10^{10}] cm^3 mol^{-1} yr^{-1}.

CH_4 becomes inaccessible to microbial degradation once it solidifies into immobile CH_4 gas hydrates, which forms when high concentrations of CH_4 meet high pressures and low temperatures. Here we assume that the saturation concentration is 50 mM assuming T=0 ˚C, S=0 PSU and a pressure equivalent to 600 m of ice thickness above the sediments, which is an average ice thickness above marginal subglacial sediments.

3.7 Global sensitivity analysis

To assess the sensitivity of CH_4 fluxes and OPD from/in subglacial sediments to variations in model parameters, we used the 'Elementary Effect Test' (Morris, 1991; Saltelli et al., 2007), which takes the mean of finite differences as a measure of global sensitivity of input parameter i:

$$S_i = \frac{1}{r}\sum_{j=1}^{r} EE^j = \frac{1}{r}\sum_{j=1}^{r} \frac{g(\chi_1^j,\ldots,\chi_i^j+\Delta_i^j,\ldots,\chi_M^j) - g(\chi_1^j,\ldots,\chi_i^j,\ldots,\chi_M^j,)}{\Delta_i^j} c_i$$

Where $g()$ is our diagenetic model, which transforms the vector of the input factors $\chi^j = (\chi_1^j,\ldots,\chi_M^j)$ into the output space - specifically the simulated CH_4 fluxes and OPD at the sediment-water/ice interface. Δ_i represents the variation of the input parameter i (i.e. sediment thickness, subglacial OM concentration, and its reactivity, dissolved O_2 at the sediment-water/ice interface and aerobic methanotrophic activity) and output j. We calculate the standard deviation of the EEs, which measures the degree of interaction of input parameter i with the other input parameters. Both sensitivity indices are relative measures, hence their values do not have a specific meaning and are only used to rank the influence of the input parameters.

To compute the mean and standard deviation of the EEs for M input parameters (M = 5), a total of N = r·(M + 1) model evaluations are required. To evaluate the robustness of the sensitivity indices and determine whether they are independent of the specific input-output sample, we derived bootstrapping-based confidence limits for the indices. Following recommendations in the literature (r>30, e.g., Pianosi et al., 2016), we computed r = 35 finite differences, a number sufficient

https://doi.org/10.5194/egusphere-2025-5506
Preprint. Discussion started: 23 December 2025

to distinguish between influential and non-influential parameters and to estimate reasonable confidence intervals for the sensitivity indices (Pianosi et al., 2016). Overall, for our global sensitivity analysis (GSA) we conducted N = r·(M + 1) = 210 model simulations using varying input parameter values.

3.8 Setup for two case studies in SW Greenland

The model-derived subglacial sediment CH_4 fluxes generated across the entire range of environmental conditions (i.e., OM content and reactivity, sediment depth, and redox conditions) establish quantitative relationships between environmental parameters and resulting CH_4 fluxes, effectively creating a multidimensional response function. Comparing the observed laterally transported CH_4 with the simulated subglacial sediment CH_4 fluxes helps identify the combinations of OM availability, reactivity, sediment thickness, and oxygen availability that could reproduce the measured signal. Thus, the modelled CH_4 fluxes serve as a quantitative diagnostic framework for constraining the range of plausible subglacial environmental conditions, including the minimum OM content and its reactivity consistent with observed CH_4 export under various assumptions of catchment sediment cover.

We use the well-studied glaciers of Isunnguata Sermia (IS) and Leverett Glacier (LG) (SW Greenland) to illustrate in our case studies to extrapolate diffusive subglacial sediment CH_4 fluxes out of subglacial sediments into seasonal lateral fluxes and dissolved CH_4 concentrations in meltwater (Fig. 5 a) for different assumptions of subglacial sediment covers and CH_4 oxidation scenarios during lateral transport, as well as their loss during lateral transport. We used modelled mean cumulative discharge between May and September 2012 - 2022 (5.5 ± 2.4 km^3 for IS; 1.4 ± 0.32 km^3 for LG, Mankoff et al., 2020) and compare our results to observed lateral CH_4 transport from these catchments measured between 2015 and 2023 (Lamarche-Gagnon et al., 2019; Hatton et al., in review, 2025).

3.9 Model Output

We applied our RTM to model key porewater and solid-phase depth profiles, and production and reduction rates of O_2 and CH_4, the integrated reaction rates and the resulting diffusive fluxes. Subsequently, we extrapolated our mass balance calculation to the IS and LG catchments and compared results to previously measured dissolved CH_4 concentrations and estimated diffusive and lateral fluxes of CH_4.

4 Results and Discussion

4.1 O_2 dynamics in subglacial sediments

Model results show that subglacial sediments in the warm-bed areas of the GrIS are predominantly anoxic, with O_2 penetration depths (OPD) ranging from 1.8-184cm and averaging 22.8 cm even with fully oxygenated overlying waters (Fig. 3). Global sensitivity analysis (GSA) results reveal that OM reactivity (parameterized by the RCM parameter ν) exerts the dominant

https://doi.org/10.5194/egusphere-2025-5506
Preprint. Discussion started: 23 December 2025

control over OPD, with OM content and aerobic oxidation of CH_4 (k_{AeOM}) playing a lesser role (Fig. 3). Highly reactive OM drives high O_2 demand through OM respiration and AeOM (see sec. 4.3), thus restricting penetration depth and favoring anoxic conditions. Conversely, less reactive OM reduces O_2 demand, enabling deeper penetration and ultimately limiting CH_4 production. When the subglacial water O_2 concentration is <50 µM (~15% saturation), OPD remains shallow (<30 cm) regardless of other sediment properties (Fig. 3). Above 50 µM, OPD scales with overlying-water O_2 deepening the oxic layer. Simulated O_2 fluxes into the sediment range from 1.6 to 240.3 mmol m^{-2} yr^{-1}, with a mean of 44.0 ± 47.0 (mean ± SD) mmol m^{-2} yr^{-1}. AeOM is an important O2 sink, accounting for up to ~67 % (0.03 – 66.9 %; 23.7 ± 18.1 %, mean ± SD) of the total O2 consumption, a process that highlights a key escape path for CH_4 through the sediment-water/ice interface. Heterotrophic respiration of OM contributes between 24.9–64.6 % (38.7 ± 9.6 %, mean ± SD).

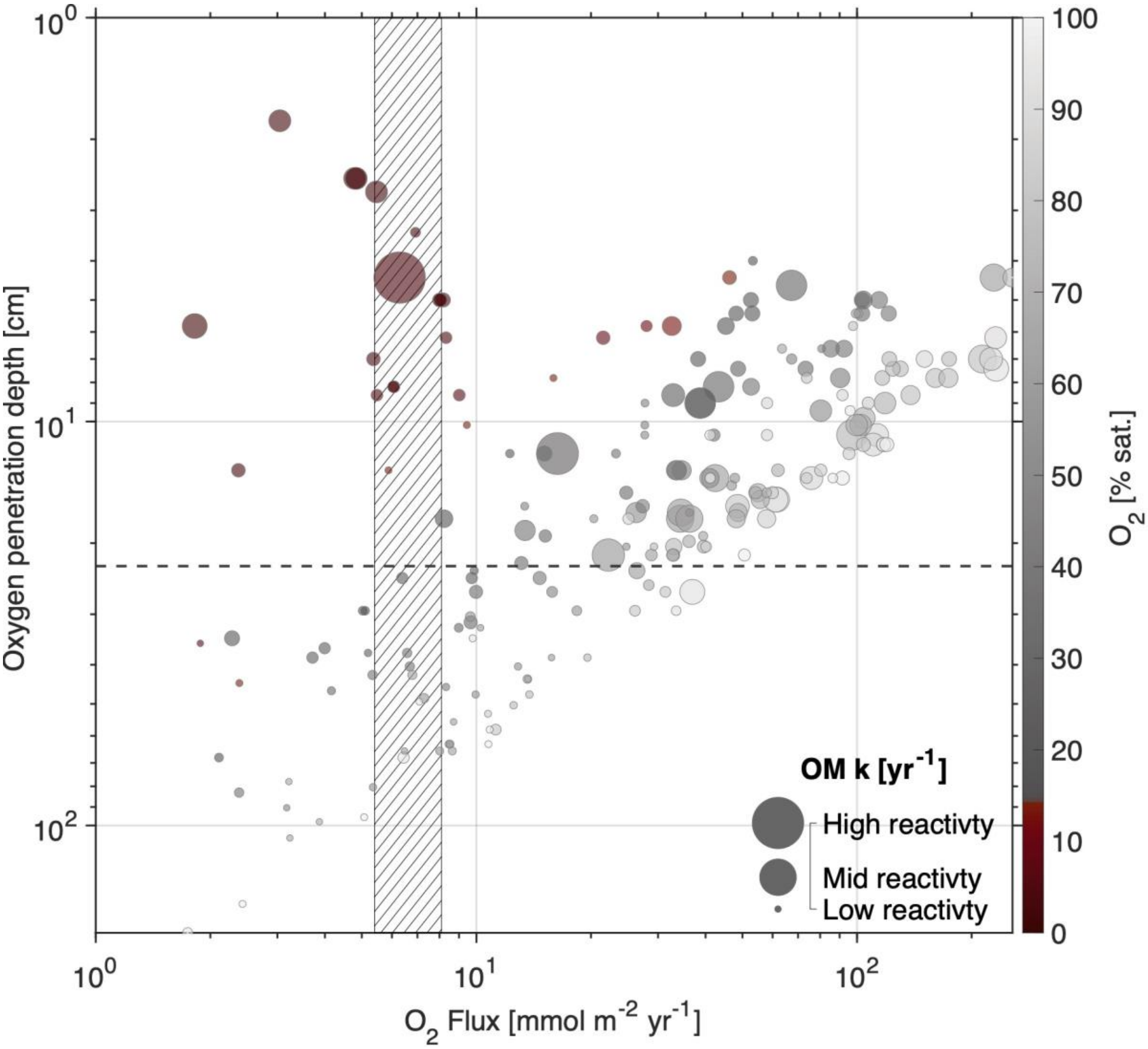

Figure 3: Modelled O_2 fluxes across the sediment-water/ice interface versus O_2 penetration depths (OPD) in GrIS subglacial sediments. Higher O_2 fluxes indicate higher microbial activity (heterotrophic respiration and/or CH_4 oxidation), reducing O_2

https://doi.org/10.5194/egusphere-2025-5506
Preprint. Discussion started: 23 December 2025

penetration. Anoxic conditions (O_2 <15% saturation, shaded in red which equates to 50 µM) are associated with shallower O_2 penetration and increased OM reactivity (OM k) (circle size). The hatched vertical bar indicates baseline O_2 flux delivered by basal melting (see sec. 3.6.5). The dashed line is the average OPD of 22.8 cm.

4.2 CH_4 production in subglacial sediment

The extensive anoxic zones within the GrIS subglacial sediment create favorable conditions for methanogenesis. Model results reveal CH_4 production rates range from 0.6×10^{-10} to 1.1×10^{-5} mol g.d.w^{-1} yr^{-1} with a mean of $(0.61 \pm 8.0) \times 10^{-7}$ mol g.d.w^{-1} yr^{-1} (mean ± SD). These rates fit the range of rates measured in incubation experiments with subglacial sediment from Greenland ($(4.5 \pm 3.7) \times 10^{-10}$ mol g.d.w^{-1} yr^{-1} (mean ± SD); Stibal et al., 2012), Canadian Arctic ($(2.3 \pm 3.3) \times 10^{-8}$ mol g.d.w^{-1} yr^{-1} (mean ± SD); Boyd et al., 2010; Stibal et al., 2012), and Antarctica ($(2.9 \pm 2.6) \times 10^{-7}$ mol g.d.w^{-1} yr^{-1} (mean ± SD); Stibal et al., 2012). Fig. 5 shows the comparison between modelled and measured rates across different studies and cryospheric environments. The highest modelled production rates are comparable to rates measured in incubation experiments of Arctic soil/sediments with much higher OM concentrations (up to 30 wt%) than those assumed here (Yedoma lakes; 3.56×10^{-4} mol g.d.w^{-1} yr^{-1}; De Jong et al., 2018, and permafrost peat soils; $5.0 \pm 4.0) \times 10^{-6}$ mol g.d.w^{-1} yr^{-1}; Kotsyurbenko et al., 2004). Results from the GSA suggest that CH_4 production rate is largely controlled by O_2 concentration, with OM content and reactivity as secondary drivers.

The model suggests that CH_4 saturation of porewaters is rarely reached and CH_4 remains thus primarily dissolved in porewater, which can diffuse upwards and become available for other microbial processes. However, immobile gas hydrates, which are a function of pressure (ice thickness above the sediments), temperature, and salinity, are present in approximately a third of our model results, formed once CH_4 exceeds saturation (50 mM; see methods), thus making up a large CH_4 pool inaccessible to microbial degradation. Depth-integrating the CH_4 production rate yields a range from 0.1 to 1600 mmol m^{-2} yr^{-1}, with a mean of 73 ± 136 mmol m^{-2} yr^{-1} (mean ± SD). Results from the GSA indicate that depth-integrated CH_4 production rates are controlled by OM reactivity, subglacial sediment depth, and OM concentration (in this order, see Fig. B1). The primary driver, OM reactivity, directly controls (together with OM concentration) the rate at which OM is transformed into CH_4 (see reaction r2 in table C1). Sediment depth indirectly influences the depth-integrated methanogenesis rate by increasing the overall thickness of the methanogenic zone; so, a thicker sediment column contains a larger anoxic zone, leading to greater total CH_4 production. Additionally, subglacial sediments less than two meters deep show a positive correlation between sediment depth and depth-integrated CH_4 production rate. However, this relationship breaks down in deeper sediments (see dotted line in Fig. 5), and the drivers (i.e., OM concentration and reactivity) gain more influence. Finally, our GSA ranks k_{AeOM} and O_2 as the weakest controls on subglacial depth-integrated CH_4 production rate.

4.3 CH_4 oxidation in subglacial sediment

AeOM is generally restricted to the uppermost tens of centimeters of sediment, where O_2 is available (i.e. above the OPD). Simulated AeOM rates span over several orders of magnitude, ranging from 1.5×10^{-18} to 3.4×10^{-6} mol cm^{-3} yr^{-1}, with mean values of $4.4 \pm 6.2 \times 10^{-7}$ (mean ± SD) mol cm^{-3} yr^{-1} for the model ensemble. Our simulated mean rates compare well to the measured rates in incubation experiments using water samples from a subglacial outflow in Greenland (1.2×10^{-7} mol cm^{-3} yr^{-1}; Dieser et al., 2014), but are two orders of magnitude higher than AeOM measured in Antarctic subglacial lake sediments (3.07×10^{-9} mol cm^{-3} yr^{-1}; Michaud et al., 2017).

AeOM rates and AeOM efficiencies (i.e. ratio of depth-integrated AeOM rate to depth-integrated methanogenesis rate) are primarily controlled by OM reactivity and k_{AeOM}; O_2 and OM contents also play a significant yet secondary role. An increase in k_{AeOM} narrows the CH_4/O_2 transition zone and shifts closer to the surface, resulting in a shallower OPD.

Across the GSA ensemble, AeOM efficiency is highly variable, ranging from near-zero to 100 %, with a mean of 51 %. AeOM efficiency is negatively correlated with OM content and its reactivity, because the rapid O_2 consumption via heterotrophic respiration reduces O_2 availability for AeOM. Conversely, k_{AeOM} and O_2 concentration are positively correlated, with k_{AeOM} exerting primary control over the oxidation efficiency. Therefore, high oxidation efficiencies within sediments (>90 %), such as those observed in Antarctic subglacial lakes (Michaud et al., 2017), are only attainable when OM reactivity is low ($\nu<0.06$), k_{AeOM} is high ($> 10^{8.8}$ cm^3 mol^{-1} yr^{-1}), and under prevailing oxic conditions ($O_2 > 50$ µM, above 15 % sat.). Sediment depth is not a primary driver of oxidation efficiency. However, across our GSA most boundary conditions lead to oxidation efficiencies much lower than the 90 % of the depth-integrated subglacial CH_4 production rate. This is particularly true for subglacial sediment characterized by low O_2 concentrations ($O_2 < 50$ µM) in overlying subglacial waters, but also for thick sediments (> 5 m) with high contents of comparatively reactive OM ($\nu \sim 0.2$). Therefore, our results indicate that GrIS subglacial sediment tends to act as a weak filter for diffusive CH_4 fluxes, and that even sediments underlying fully oxygenated waters can thus be a source of CH_4 to the subglacial drainage system, unlike for what has been observed in Antarctic subglacial lakes (Michaud et al., 2017).

4.4 Diffusive CH_4 fluxes from subglacial sediment

The imbalance between CH_4 production and consumption results in a net flux across the sediment-water/ice interface into the subglacial hydrological system, where it dissolves in meltwater (Fig. 4). Simulated fluxes range between [0 - 234.7] mmol m^{-2} yr^{-1} (Fig. 5) with mean fluxes of 33.7 ± 32.5 (mean ± SD) mmol m^{-2} yr^{-1}. The majority of the modelled fluxes exceeds calculated estimates in SW Greenland, e.g. Isunnguata Sermia (IS) 0.0024 - 0.58 mmol m^{-2} yr^{-1} (Hatton et al., in review, 2025) and Leverett Glacier (LG) span 0.289 - 0.966 mmol m^{-2} yr^{-1} (Lamarche-Gagnon et al., 2019), but are comparable to those reported for Russell Glacier (RU) 25.7 - 51.5 mmol m^{-2} yr^{-1} (Dieser et al., 2014). Diffusive fluxes for IS and RU were calculated by normalizing reported laterally transported CH_4 by the glaciers' respective total catchment area. Our modelled diffusive fluxes cover observed fluxes across a variety of different environments from Antarctic subglacial lake at 6.8 ± 1.8 mmol m^{-2} yr^{-1} (Michaud et al., 2017) to groundwater fluxes in proglacial lakes in southwest Greenland around 951.3± 2123.8 mmol m^{-2} yr^{-1} (Olid et al., 2022). The difference between our modelled fluxes and those calculated using literature data reflects methodological differences (simple mass balance vs. RTM) and underscore the difficulties of extrapolating laterally transported CH_4 to area-normalized fluxes, as done here and in Lamarche-Gagnon et al. (2019). Along with a better spatial

https://doi.org/10.5194/egusphere-2025-5506
Preprint. Discussion started: 23 December 2025

coverage of subglacial soft sediments, the acquisition of subglacial sediment cores with depth-resolved concentrations of OM and TEA would provide critical constraints to resolve this discrepancy.

GSA identifies OM reactivity as the primary control on diffusive CH_4 fluxes. OM quantity and sediment depth exert weak positive influence, whereas k_{AeOM} and O_2 concentration show a weakly inhibitory effect. Statistical analysis further reveals that the diffusive CH_4 flux is shaped by the interaction of these drivers. For instance, OM quantity and reactivity act synergistically, driving particularly large diffusive fluxes when both are high, although k_{AeOM} consistently reduces this positive effect. Conversely, the negative effect of O_2 concentration increases with depth and in combination with k_{AeOM}, but is partially offset by high OM reactivity.

In sediments shallower than 2 m, depth is positively correlated with diffusive CH_4 flux (dotted line in Fig. 5). However, this trend disappears below the maximum OPD, where anoxic conditions promote methanogenesis and upward diffusion becomes unaffected by AeOM. Interestingly, even shallow sediments (<1 m) produce diffusive fluxes large enough to cross the oxic filter (24.4 mmol m^{-2} yr^{-1}), under conditions of moderate OM quantity (0.2 wt%) with very high reactivity (ν=1.15) when k_{AeOM} is low ($10^{6.7}$ cm^3 mol^{-1} yr^{-1}), regardless of O_2 concentrations at the sediment-water/ice interface. However, most fluxes in shallow sediments (< 2 m) are lower (4.9 ± 8.1 (mean ± SD) mmol m^{-2} yr^{-1}) with low oxidation efficiencies. By contrast, sediments deeper than 2 m that contain OM of very low reactivity cannot produce sufficient CH_4 to overcome oxidative losses, thus limiting the CH_4 flux into subglacial meltwater. These results demonstrate that while sediment depth is relevant, OM remains the strongest driver of diffusive CH_4 flux.

https://doi.org/10.5194/egusphere-2025-5506
Preprint. Discussion started: 23 December 2025

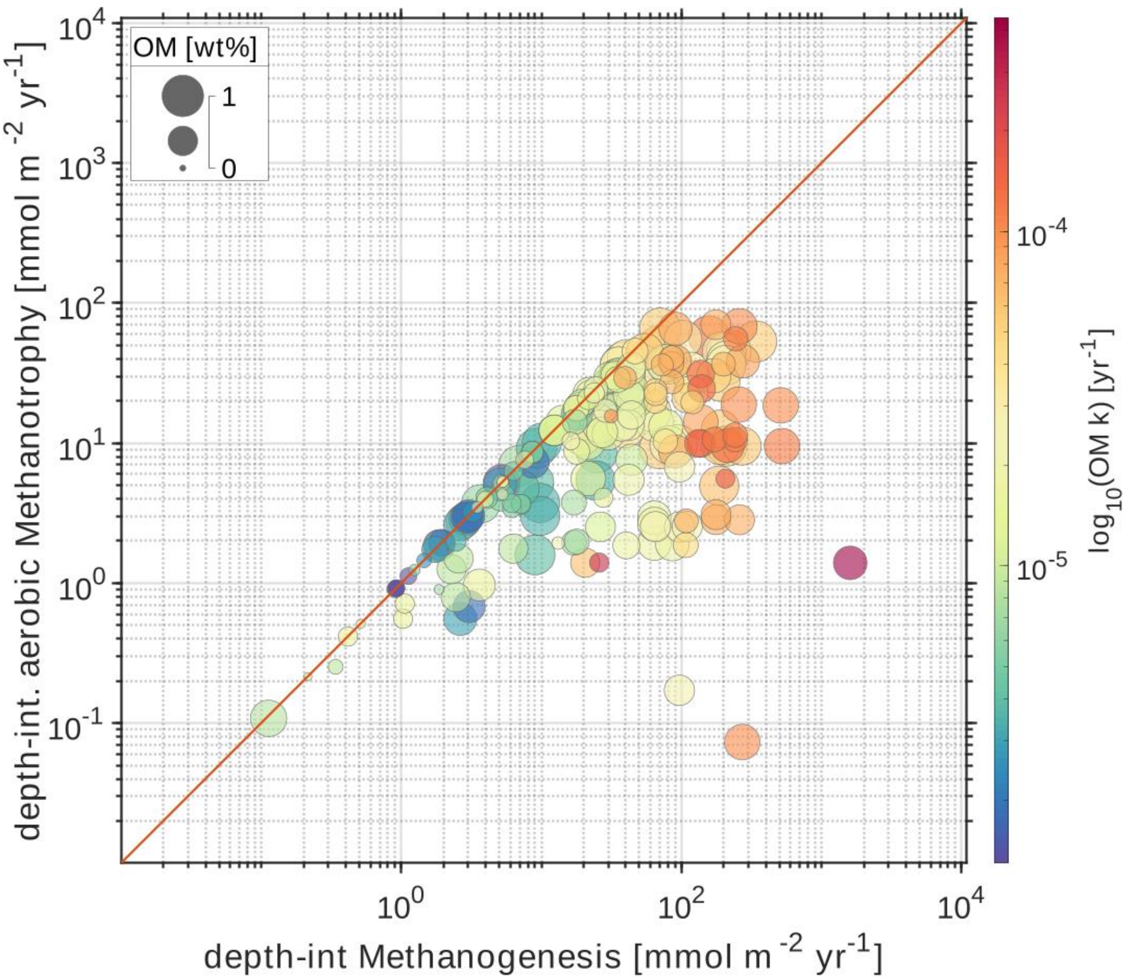

Figure 4: Scatter plot illustrating the relationship between CH_4 production and consumption, with bubble size representing OM content and color indicating reactivity (OM k). The 1:1 line indicates that depth-integrated CH_4 production rates equal consumption rates, which prevents diffusive flux across the sediment-water interface.

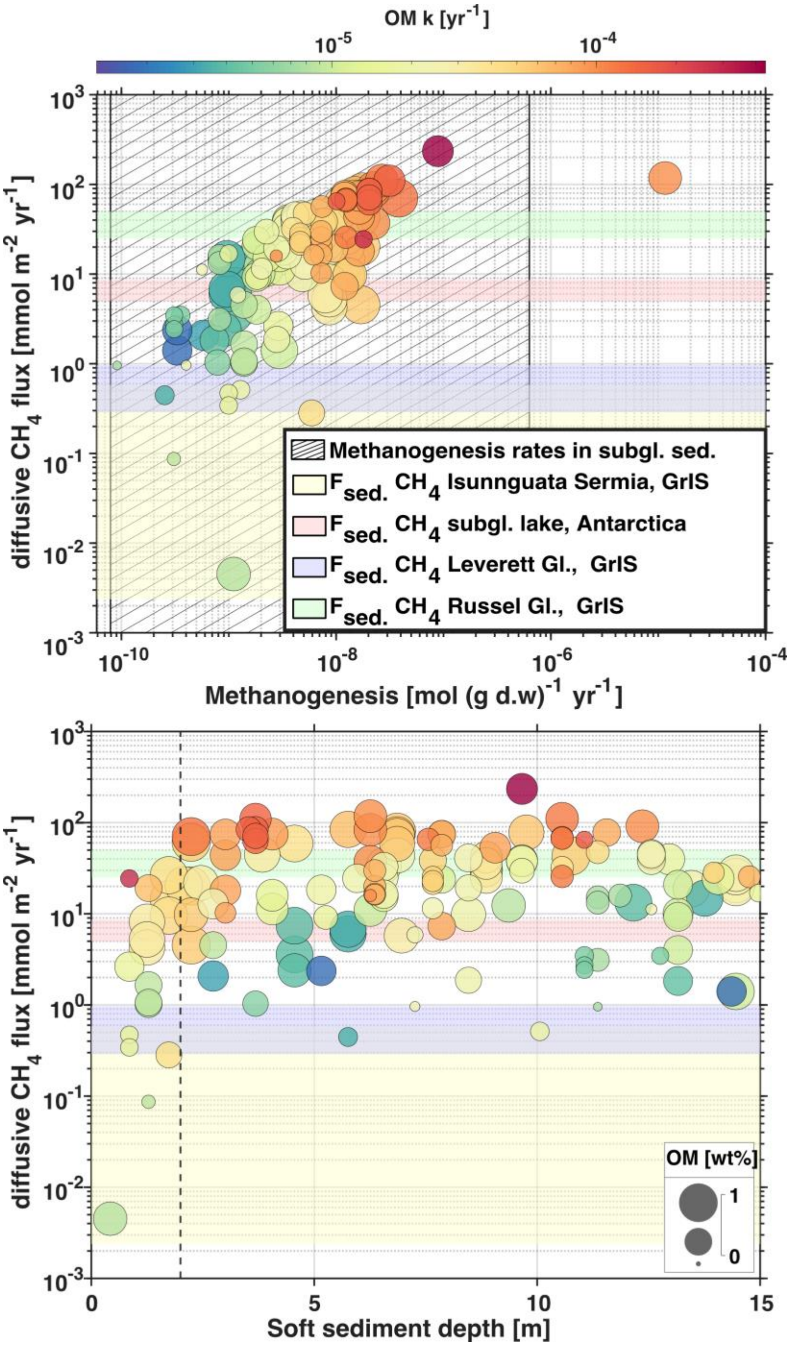

Figure 5: Modelled results for diffusive CH_4 flux out of the subglacial sediment as functions of sediment depth (left panel) and rate of methanogenesis (right panel). Left: Main drivers of simulated diffusive CH_4 flux from subglacial sediments into the subglacial environment. OM reactivity (denoted as OM k, circle color) is the strongest driver, followed by OM content (circle size), and sediment depth (x-axis). Sediment depth of less than 2 m drives CH_4 flux, whereas deeper sediments exert no significant influence.

Right: Simulated methanogenesis rates driving diffusive CH_4 flux. Simulated rates are compared to measured rates and fluxes through the sediment-water interface (SWI) from various cryospheric environments. The grey shaded area is the range in measured methanogenesis rates from incubation experiments from glaciers in Greenland, Antarctica, and Canada (Boyd et al., 2010; Stibal et al., 2012). Horizontal colored areas show comparative diffusive fluxes from sediments in a subglacial lake in Antarctica (Michaud et al., 2017), and extrapolated/calculated area yield fluxes (i.e. lateral export divided by reported catchment area) in GrIS at Isunnguata Sermia (Hatton et al., in review, 2025), Leverett Glacier (Lamarche-Gagnon et al., 2019), and Russell Glacier (Dieser et al., 2014).

4.5 Inferring subglacial environmental conditions: A case study on Isunnguata Sermia and Leverett Glacier (SW Greenland)

The comparison of simulated and measured CH_4 concentrations in subglacial meltwater ($CH_{4(aq)}$) allows inferring plausible combinations of subglacial environmental conditions within the catchment areas, able to sustain observed lateral CH_4 fluxes from two well-studied outlets of the SW GrIS (IS and LG). To this end, we estimate the potential lateral CH_4 fluxes by combining modelled diffusive sediment fluxes with hydrological scaling, oxidation, and off-gassing rates.

IS and LG drain catchments of approximately 14,000 km^2 and 1200 km^2, respectively (Mankoff et al., 2020). However, the hydrologically active subglacial areas are likely much smaller, yet critical for upscaling and estimating lateral fluxes. For instance, LG is thought to have a hydrologically active subglacial area approximately half its full catchment size (Cowton et al., 2012; Hawkings et al., 2021). Because glacier surface slope drives the hydraulic gradient, the surface catchment provides a first-order approximation of subglacial meltwater routing (Palmer et al., 2011; Cowton et al., 2012). Based on this approach, Cowton et al. (2012) put the active area at 600 km^2 at LG, while we estimated ~1300 km^2 at IS. However, the extent to which these areas are underlain by soft sediment remains unknown.

We then spatially upscale the simulated sediment CH_4 fluxes (0 - 234.7 mmol m^{-2} yr^{-1}) to fractions of the hydrologically active and total area assumed to be underlain by subglacial sediments (see Fig. 6 a-b). Under these assumptions, IS could produce lateral fluxes of 0.03 - 3.3 × 10^9 mol CH_4 (0.39 - 39.5 Gg) per year, while LG 0.0028 - 0.27 × 10^9 mol CH_4 (0.0339–3.4 Gg) per year, and are comparable to lateral fluxes in the proglacial rivers at both sites of 0.002-28.9 Mg per year (IS; Hatton et al. in review) and 2.8 - 9.3 Mg per year (LG, Lamarche-Gagnon et al., 2019). Multiplying the lateral flux with annual discharge (IS: 5.5 ± 2.4 km^3 yr^{-1}; LG: 1.4 ± 0.32 km^3 yr^{-1}; see Mankoff et al., 2020), results in average dissolved CH_4 concentrations in meltwaters over a season ranging between 0.0001 - 593.4 µM for IS and 0.0003 - 200.2 µM for LG. These results suggest that dissolved CH_4 concentrations in meltwater are similar despite the generally large difference in catchment size.

Depending on the soft sediment cover present in the hydrologically active catchment area, the simulated $CH_{4(aq)}$ may exceed, match, or fall below measured $CH_{4(aq)}$ in proglacial rivers at the glacier outlet (see grey shading in Fig. 6 a-b; IS: 0.006–0.13 µM (Hatton et al., in review, 2025); LG: 0.036 - 0.7 µM (Lamarche-Gagnon et al., 2019)). In a few cases, the simulated $CH_{4(aq)}$ falls below the measured $CH_{4(aq)}$, meaning such combinations of OM, sedimentary characteristics, and sediment cover are unlikely to result in measurable $CH_{4(aq)}$ at the glacier margin. However, in cases where the simulated $CH_{4(aq)}$ fall within the observed range, we postulate that no or minimal CH_4 oxidation or off-gassing occurs during lateral transport in the subglacial

https://doi.org/10.5194/egusphere-2025-5506
Preprint. Discussion started: 23 December 2025

hydrological system. Fig. 6 a-b shows that even a low subglacial sediment coverage (i.e., < 1% and <10% of the hydrologically active area), with a modest concentration (~0.5 wt%) of relatively unreactive (ν > 0.02) OM supports observed CH_4 concentrations. In contrast, exceeding observed concentrations requires OM with either higher OM content (~0.65 wt%) and/or higher reactivity (ν > 0.14), which in turn implies a loss of CH_4 before reaching the glacier outlet, either by in-stream oxidation or off-gassing. If we instead assume a 10% coverage of subglacial sediment, 78% for IS and 56% for LG of simulated $CH_{4(aq)}$ exceed observed $CH_{4(aq)}$, suggesting additional removal processes. Simulated $CH_{4(aq)}$ exceeding measured ranges (IS: 0.13 - 6 µM, LG: 0.7 - 10 µM) imply substantial subglacial in-transit losses, possibly through microbial oxidation and/or off-gassing. Fig. 6 c-d highlights the necessary OM concentration and reactivity to produce such excess $CH_{4(aq)}$ (circles with white border). Conversely, some combinations of boundary conditions result in $CH_{4(aq)}$ within the measured range (circles with blue border), indicating no or minimal loss during lateral transport to the glacier outlet. Finally, if sediment covers more than 50% of the active hydrological area, almost all estimated concentrations (even for low OM and low reactivity) exceed observed concentrations.

These findings highlight that even limited subglacial sediment coverage and low contents of relatively unreactive OM already suffice to support observed subglacial $CH_{4(aq)}$. Because subglacial sediment cover is likely above 1%, they also suggest that a fraction of the CH_4 produced in subglacial sediments is either stored in the subglacial environment or is oxidized or evades during transport in the subglacial hydrological network. Estimating the potential extent of additional CH_4 oxidation in the subglacial hydrological network will further help delineate the subglacial sediment cover, OM content and reactivity required to support observed concentrations and fluxes.

To this end, we postulate that $CH_{4(aq)}$ is rapidly consumed in the channel's sediments in a process similarly observed in proglacial streams (Lamarche-Gagnon et al., 2019; Strock et al., 2024). We use an oxidation rate reported from a nearby subglacial environment (0.32 µM day^{-1}; Dieser et al., 2014) to calculate how quickly the excess $CH_{4(aq)}$ at IS (6 µM) and LG (10 µM) decreases to the observed levels (Fig. 6 e-f). Because $CH_{4(aq)}$ oxidation is time-dependent, we use the meltwater residence time from LG, which ranges from hours near the outlet to several days further upstream (grey shading in Fig. 6 e-f; Chandler et al., 2013). We combine these assumptions to model to focus on modelled $CH_{4(aq)}$ exceeding measured concentrations resulting from 10 % subglacial sediment cover under the hydrologically active area and simulate their O_2-unconstrained oxidation during transit in the channelized drainage system. Fig. 6 e-f illustrates that $CH_{4(aq)}$ are still above observed $CH_{4(aq)}$ by the time the melt water exits the subglacial environment, suggesting that oxidation does not suffice as CH_4 sink within the subglacial system. To remain within the observed $CH_{4(aq)}$ and the residence time of 72 hours, soft sediments under IS would have to produce fluxes ranging from 5.9 to 7.4 mmol m^{-2} yr^{-1} and at LG 16.8 - 41.0 mmol m^{-2} yr^{-1}. In both catchments, sediments should be deep (9.2 ± 3.6 m) and have substantial OM concentrations (0.64 ± 0.27 wt%) of low reactivity (ν=0.15 ± 0.1 for IS and ν=0.08 ± 0.12). Higher OM reactivity (ν=0.22 ± 0.22 at LG and ν=0.37 ± 0.3 at LG) would yield $CH_{4(aq)}$ concentrations exceeding measured values even after 72 hours of water residence time, suggesting out-gassing or higher oxidation rates are required.

The results point to several key implications for subglacial CH_4 cycling. First, CH_4 fluxes from subglacial sediments in SW GrIS may be substantially larger than previously calculated, with the spatial extent of soft sediments in hydrologically active zones acting as a critical control. The sensitivity of modelled $CH_{4(aq)}$ to assumptions about sediment cover highlights the need for direct mapping of subglacial sediment beneath the margins of major GrIS catchments. Secondly, in-stream CH_4 loss depends strongly on the assumed oxidation rate, which may vary seasonally as methanotrophs adapt to substrate availability (i.e. due to seasonal changes in $CH_{4(aq)}$ concentrations from changes in dilution from supraglacial meltwaters). Additionally, in-stream CH_4 loss via evasion through turbulent flow around the glacier outlet might substantially increase the required diffusive CH_4 flux and in turn the CH_4 production in subglacial sediments to match the observed range. Because we do not account for this process, our flux estimates are likely conservative. Third, hydrological constraints, through their control on water residence time, emerge as a first-order determinant of whether CH_4 is preserved or oxidized before reaching the margin. Fourth, while we do not currently account for off-gassing as meltwater travels within the unpressurised drainage system (Chandler et al., 2013), we recognize that it may represent a significant loss of CH_4 during lateral transport. We hypothesize that in glacier hydrological systems characterised by upwelling, where meltwater surges at the glacier front, i.e. Isunnguata Sermia, subglacial pressurization changes may drive and redirect evaded CH_4 towards marginal outlets where high(er) CH_4 concentrations ($CH_{4(aq)}$ = 5 µM) have been recorded (e.g. Christiansen and Jørgensen, 2018). As such, $CH_{4(aq)}$ measurements at the upwelling might not fully capture the entirety of the subglacially produced CH_4. We hypothesize that (seasonal) hydrological pressure changes might reroute CH_4 to lateral/marginal outlets (e.g. Christiansen and Jørgensen, 2018) and therefore that lateral fluxes measured at the main glacial outlets and in proglacial rivers may underestimate the overall CH_4 fluxes.

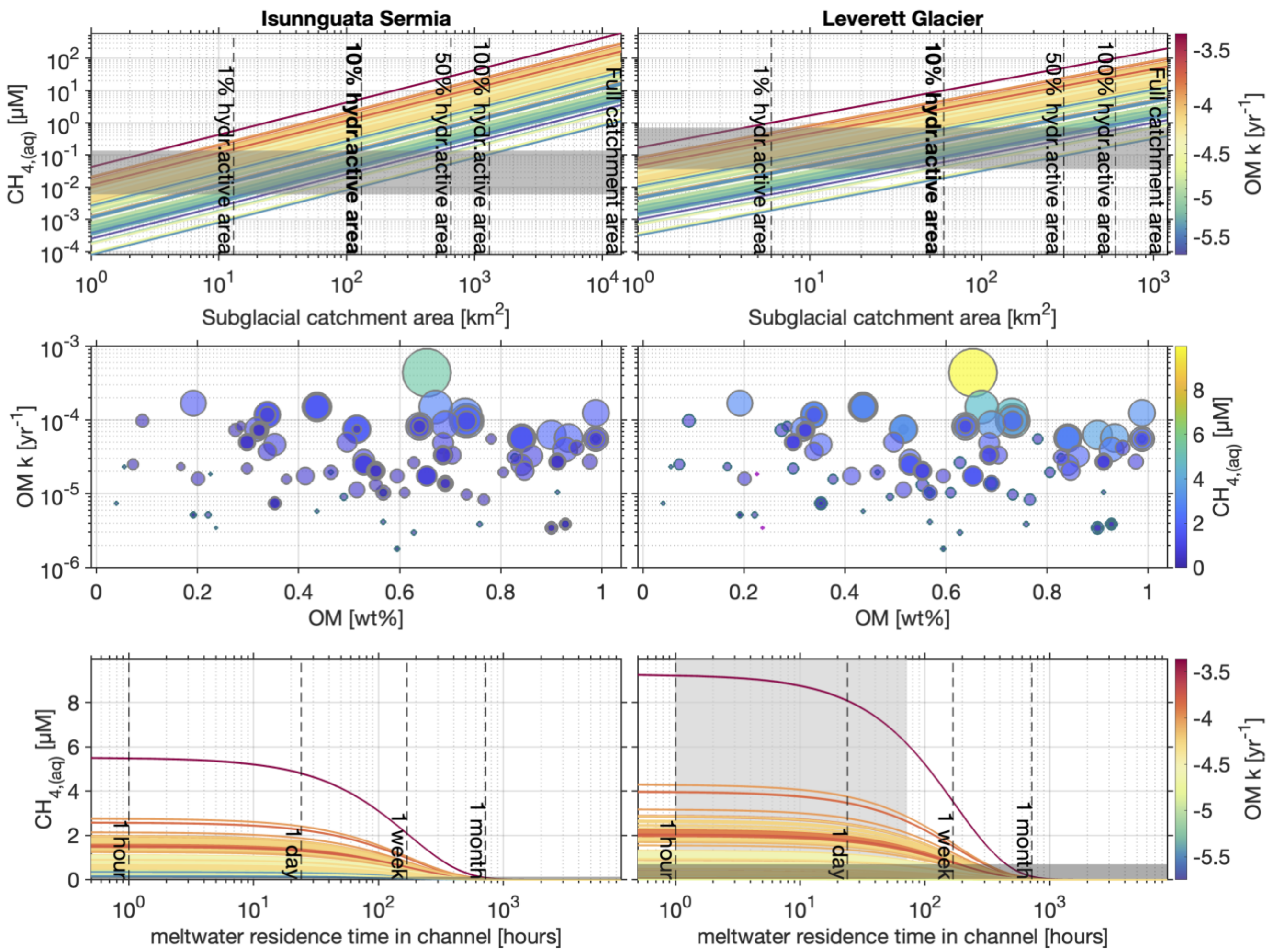

Figure 6: Case studies at Isunnguata Sermia and Leverett Glacier, Southwest Greenland, to estimate the fate of dissolved CH_4 once it enters the subglacial drainage system. Top row: in-stream CH_4 concentrations (discharge-weighted and extrapolated to increasingly hydrologically active catchment areas) leaving the glacier margin, its main drivers and its subsequent loss (oxidation) during lateral transport reaching the glacier outlet. Line color denotes OM reactivity. Grey areas are measured dissolved CH_4 concentrations in the proglacial rivers at the glacial outlets of IS (Hatton et al., in review, 2025), and LG (measurements at 1.5 km from the margin) (Lamarche-Gagnon et al., 2019). Middle row: subdivision of main drivers (OM concentration and its reactivity) by CH_4 concentration depending on whether it is above (grey-border circles), within (green-border circles) or below (magenta-border circles) site-specific measurements. Bottom row: melt water residence time vs. melt water CH_4 concentration as it decreases due to in-stream oxidation. Vertical light grey area indicates the range of residence times of meltwater at LG (Chandler et al., 2013), while horizontal dark grey area indicates the site-specific measurements.

https://doi.org/10.5194/egusphere-2025-5506
Preprint. Discussion started: 23 December 2025

5 Conclusion and future outlook

In this study, we used a reaction-transport model approach to conduct an environmental parameter sensitivity study. This approach established a quantitative framework that provides information on the magnitude and controls of subglacial CH_4 production and release and thus allows contextualizing measured CH_4 in meltwater outflow.

Our results indicate that subglacial sediments remain largely anoxic ($z > 23$ cm) even under fully O_2-saturated waters. Aerobic oxidation of methane (AeOM) efficiency—defined as the ratio of depth-integrated AeOM to methanogenesis—varies from nearly 0 to 100 % (mean = 51 %), reflecting its strong dependence on organic matter (OM) availability and reactivity. Sediments rich in highly reactive OM exhibit low AeOM efficiency, whereas less abundant or less reactive OM yields higher efficiency. Thus, sediments with limited or less reactive OM generate and release less CH_4 overall. When subglacial water O_2 concentrations drop below 50 µM (~15 % saturation), the OPD remains shallow (< 30 cm) regardless of sediment characteristics; above this threshold, OM reactivity becomes the dominant control.

The GSA identifies OM reactivity as the primary control on diffusive CH_4 fluxes. OM quantity and sediment depth exert a weak positive influence, whereas k_{AeOM} and O_2 concentration show a weakly inhibitory effect. Depth is positively correlated with diffusive CH_4 flux in sediments shallower than 2 m, but at greater depths, low-reactivity OM limits CH_4 production and prevents fluxes from overcoming oxidative losses. Thus, while sediment depth contributes to flux variability, OM reactivity ultimately dominates. These dynamics emphasize that CH_4 fluxes emerge from coupled biogeochemical controls rather than isolated parameters.

Nevertheless, our sensitivity study shows that nearly one-quarter of parameter combinations yield negligible CH_4 flux, even when conditions appear favorable (e.g. deep anoxic sediments). Our simulated sediment CH_4 fluxes range from 0 to 234.7 mmol m^{-2} y^{-1} (Fig. 5), with mean fluxes of 33.7 ± 32.5 mmol m^{-2} y^{-1} (mean ± SD). Most modeled fluxes exceed calculated estimates for southwestern Greenland, including Isunnguata Sermia (0.0024–0.58 mmol m^{-2} y^{-1}; Hatton et al., in review, 2025) and Leverett Glacier (0.289–0.966 mmol m^{-2} y^{-1}; Lamarche-Gagnon et al., 2019), but are comparable to values reported for Russell Glacier (25.7–51.5 mmol m^{-2} y^{-1}; Dieser et al., 2014).

This work also reveals a critical biogeochemical trade-off governing net CH_4 export. Based on the case studies at Isunnguata Sermia and Leverett Glacier (SW GrIS), achieving previously reported CH_4 export (Lamarche-Gagnon et al., 2019; Hatton et al., in review, 2025) requires a narrow balance of conditions. While high OM reactivity drives methanogenesis, it also promotes rapid O_2 consumption via heterotrophic respiration (by offering an easily degradable source of substrate) and CH_4 oxidation. Consequently, simulations approximating measured CH_4 concentrations in meltwaters at glacier termini emerge from a very specific set of boundary conditions, i.e., sediment layers of 9 ± 3 m, moderate OM content (0.64 ± 0.27 wt%), and low OM reactivity (ν = 0.08–0.15), permitting methanogenesis to outpace oxidation. In contrast, shallow sediments (< 1 m) are unlikely to be significant CH_4 sources, unless rich in highly reactive OM ($\nu > 1.0$).

Our analysis provides a first-order approximation by focusing on biogeochemical processes within the static sediment column. The model neglects several potentially important redox processes (iron and nitrate cycles), which likely influence CH_4 cycling.

Additionally, a more sophisticated formulation of the transport and transformation of CH_4 within the dynamic subglacial hydrological system is a likely candidate for improvement. The model also neglects transient processes, including seasonal hydrological flushing, sediment erosion, and changes in O_2 supply, which likely constitute an additional control over the CH_4 emissions. Such processes also differentiate the GrIS environments from Antarctic subglacial lakes, where stagnant, O_2-rich waters sustain > 90% oxidation.

These findings reveal the critical consequences for subglacial exploration, indicating that drilling strategies should prioritize areas with deep sediment to locate active methanogenic communities and their substrates. Additionally, future modelling work would also greatly benefit from depth-resolved measurements of solid and dissolved species, such as OM and terminal electron acceptors (e.g., sulfate and bioavailable iron) to expand our reaction network and, thus, our understanding of subglacial biogeochemistry. And finally, future work should also integrate reactive transport with subglacial hydrology to capture CH_4 cycling and quantify its contribution to the global CH_4 budget.

Code and data availability. Boundary conditions for the Global sensitivity analysis and model output Model outputs are available from the Zenodo repository: https://doi.org/10.5281/zenodo.17512276

Author contributions. PA, MS and SA conceived the idea. PP built, implemented and performed model runs, created the figures, and did the data curation. PP wrote the paper with guidance from MS and SA. MS and SA acquired funding. GLG and PK provided input data and field expertise for the discussion. All authors reviewed and edited the paper.

Competing interests. The authors declare that they have no conflict of interest.

Acknowledgements. We thank Dr. Jade Hatton for their careful reading and valuable comments for the revision of this paper.

Financial support. This research was funded by the Czech Ministry of Education as part of the ERC-CZ programme (project LL2004 'MARCH4G' to MS. SA was supported by EU H2020 Nunataryuk, ARC (NuTTI) and ULB strategy grant. G.L.G. is part of iC3: Centre for ice, Cryosphere, Carbon and Climate and supported by the Research Council of Norway through its Centres of Excellence funding scheme, project number 332635.

https://doi.org/10.5194/egusphere-2025-5506
Preprint. Discussion started: 23 December 2025

Appendix A: Examples of depth-profiles of concentration and rate for relevant species/rates as model output

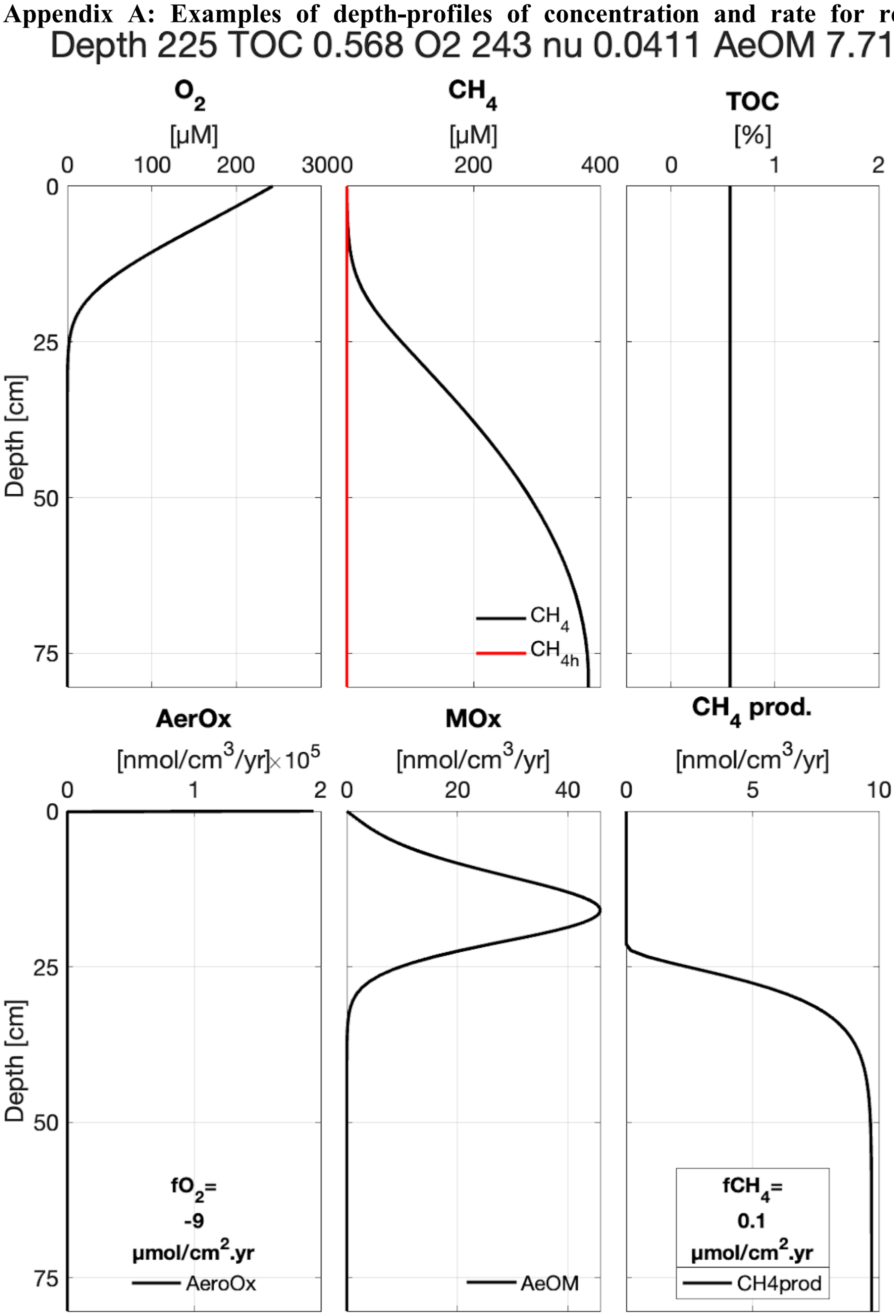

Figure A1: Depth-profiles for (constant) OM, for dissolved species and for porosity for shallow subglacial sediment depths (0.75m). Top: concentration profiles for the key species. Bottom: rate profiles. Panel on right hand side is the superposition of the primary redox reaction rates normalized by their total contribution to OM degradation.

https://doi.org/10.5194/egusphere-2025-5506
Preprint. Discussion started: 23 December 2025

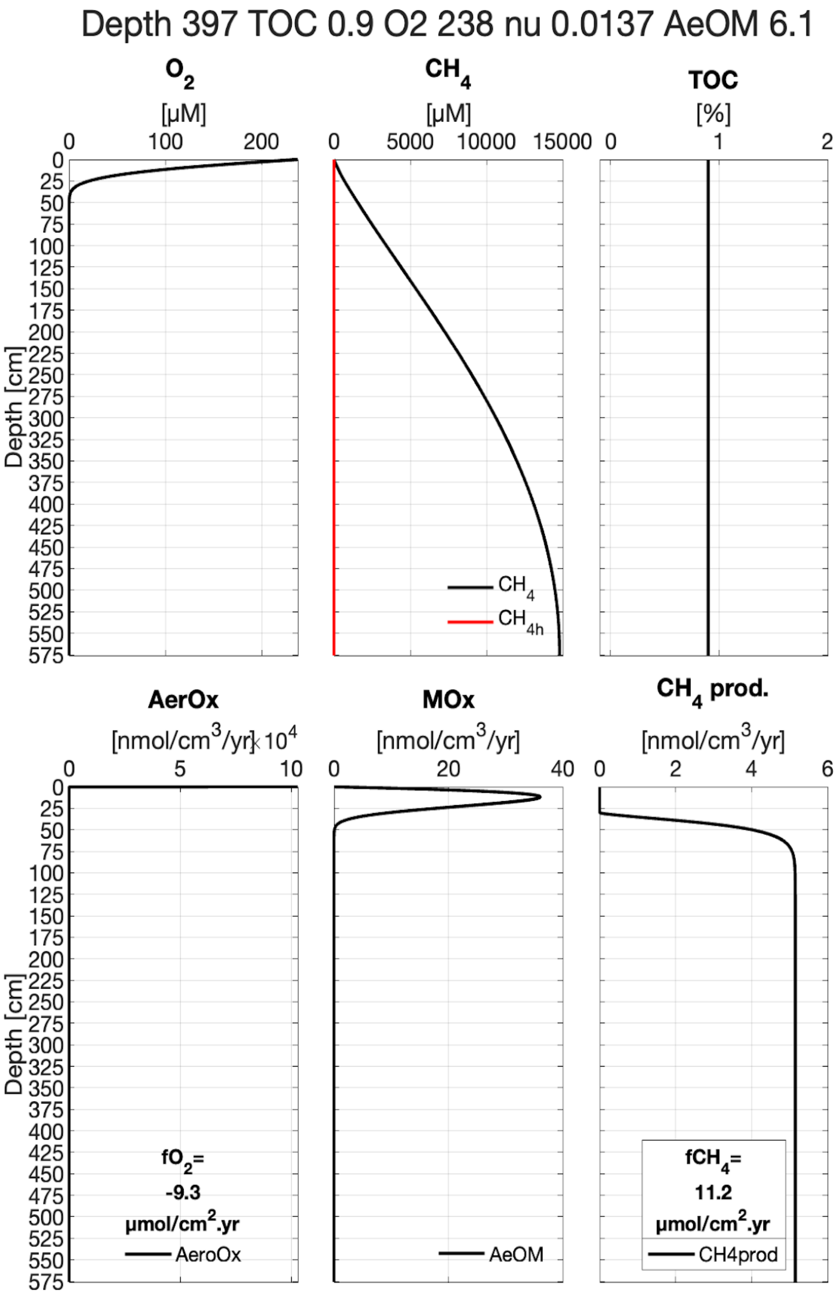

Figure A2: Depth-profiles for (constant) OM, for dissolved species and for porosity for shallow subglacial sediment depths (5.75 m). Top: concentration profiles for the most important species. Bottom: rate profiles. Panel on right hand side is the superposition of the primary redox reaction rates normalized by their total contribution to OM degradation.

https://doi.org/10.5194/egusphere-2025-5506
Preprint. Discussion started: 23 December 2025

Appendix B: Sensitivity analyses for diffusive CH4 flux and oxygen penetration depth

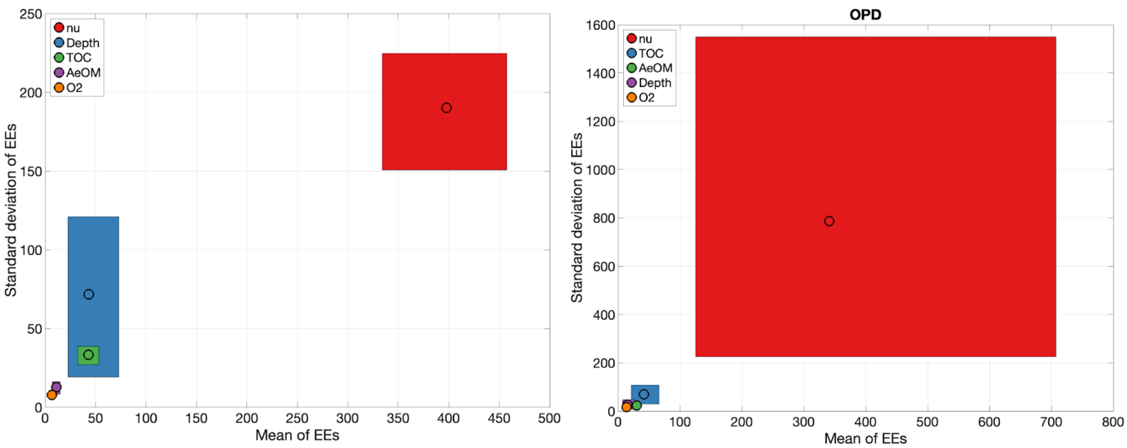

Figure B1: Sensitivity analyses for diffusive CH_4 flux out of the sediment (left panel) and for oxygen penetration depth into the sediment (right panel). Mean of Elementary Effects (EEs) versus their standard deviation for five key model parameters: nu = ν is one of the two RCM reactivity parameters, depth represents the subglacial sediment depth, TOC denotes the OM quantity, AeOM is the rate constant for the aerobic oxidation of CH_4, and O2 is the oxygen concentration at the SWI. Confidence bounds were derived via bootstrapping around the mean and standard deviation of the EEs.

Appendix C: Reaction network and list of symbols used for the model

https://doi.org/10.5194/egusphere-2025-5506
Preprint. Discussion started: 23 December 2025

664 Table C1: Reaction network governing heterotrophic organic matter degradation and CH_4 oxidation in subglacial sediments
665 implemented in the Reaction-Transport Model (Adapted from Aguilera et al., 2005; Thullner et al., 2009).

Reaction Pathway	Stoichiometry	Reaction rate
	Primary redox reactions	
Aerobic OM degradation (r1)	$(CH2O)_x(NH3)_y(H3PO4)_z + (x+2y)O2 \quad +(y+2z)HCO3-> \quad (x+y+2z)CO_2 + yNH_4^+ + zHPO_4^{2-} +(x+2y+2z)H_2O$	$r1 = \frac{\nu}{(a+age)} \cdot CH_2O \cdot fO_2$
Methanogenesis (r2)	$(CH2O)_x(NH3)_y(H3PO4)_z + (y-2z)H_2O)-> \frac{x-2y+4z}{2}CO_2 + (y-2z)HCO_3^- + yNH_4^+zPO_4^{2-} + \frac{x}{2}CH_4$	$r2 = \frac{\nu}{(a+age)} \cdot CH_2O \cdot fCH_4$
	Secondary reaction	
CH_4 oxidation by O_2	$CH_4 + 2O_2 \rightarrow CO_2 + 2H_2O$	$r3 = kAeOM \cdot CH_4 \cdot O_2$
CH_4 dissolution	$kdis \quad [CH_4(h)]([CH_4] - [CH_4]*) \quad if\ [CH_4] < [CH_4]*$ $0 \quad if\ [CH_4] > [CH_4]*$	
CH_4 hydrate formation	$khyd \quad ([CH_4] - [CH_4]*) \quad if\ [CH_4] > [CH_4]*$ $0 \quad if\ [CH_4] < [CH_4]*$	

666
667
668 Table C2: Reaction parameter values implemented in the RTM. Effective molecular diffusion coefficients (D_i) are given for
669 T = 0 °C and are corrected by subglacial environment specific temperature, salinity, and tortuosity. GSA input parameters are
670 highlighted in **bold**.

Parameter	Unit	Value	Reference
Subglacial sediment depth	m	1 - 15	This study
x/y/z	–	106/16/1	Redfield (1934)
TOC	wt%	0.02 — 1	This study; Yde et al. (2010); Stibal et al. (2012)
RCM ν	–	0.005 - 1.7	Boudreau and Ruddick (1991)
RCM a	yr	0.2	Boudreau and Ruddick (1991)
age	yr	4000	Hatton et al. In review

O_2	µM	0 - 456	This study
kAeOM	M yr	10^6 - 10^{10}	Dieser et al. (2014); Murguia-Flores et al. (2018)
D(O_2), µO2	cm^2 yr	380.45, 0.06	Wang and Van Cappellen (1996)
D(CH_4) µCH4(g)	cm^2 yr	5000.0, 0.0	Wang and Van Cappellen (1996)
$[CH_4]*$	mM	59.36	This study; calculated for 600 m ice thickness
kdis	cm^3 mol^{-1} yr^{-1}	0	Wang and Van Cappellen (1996)
khyd	yr^{-1}	789.0	Puglini et al. (2019)

References

Adnew, G.A. et al. (2025) "Clumped isotope measurements reveal aerobic oxidation of methane below the Greenland ice sheet," Geochimica et Cosmochimica Acta, 389, pp. 249–264. Available at: https://doi.org/10.1016/j.gca.2024.11.009.

Aguilera, D.R. et al. (2005) "A knowledge-based reactive transport approach for the simulation of biogeochemical dynamics in Earth systems: EARTH SYSTEM DYNAMICS," Geochemistry, Geophysics, Geosystems, 6(7), pp. n/a–n/a. Available at: https://doi.org/10.1029/2004GC000899.

Arndt, S. (in review, 2025) "On the reactivity of organic matter in Boreal and Arctic Regions," In review [Preprint].

Bhatia, M.P., Kujawinski, E.B., et al. (2013) "Greenland meltwater as a significant and potentially bioavailable source of iron to the ocean," Nature Geoscience, 6(4), pp. 274–278. Available at: https://doi.org/10.1038/ngeo1746.

Bhatia, M.P., Das, S.B., et al. (2013a) "Organic carbon export from the Greenland ice sheet," Geochimica et Cosmochimica Acta, 109, pp. 329–344. Available at: https://doi.org/10.1016/j.gca.2013.02.006.

Bierman, P.R. et al. (2014) "Preservation of a Preglacial Landscape Under the Center of the Greenland Ice Sheet," Science, 344(6182), pp. 402–405. Available at: https://doi.org/10.1126/science.1249047.

Bierman, P.R. et al. (2024) "Plant, insect, and fungi fossils under the center of Greenland's ice sheet are evidence of ice-free times," Proceedings of the National Academy of Sciences, 121(33), p. e2407465121. Available at: https://doi.org/10.1073/pnas.2407465121.

Blard, P.-H. et al. (2023) "Basal debris of the NEEM ice core, Greenland: A window into sub-ice-sheet geology, basal ice processes and ice-sheet oscillations," Journal of Glaciology, 69(276), pp. 1011–1029. Available at: https://doi.org/10.1017/jog.2022.122.

Booth, A.D. et al. (2012) "Thin-layer effects in glaciological seismic amplitude-versus-angle (AVA) analysis: Implications for characterising a subglacial till unit, Russell Glacier, West Greenland," The Cryosphere, 6(4), pp. 909–922. Available at: https://doi.org/10.5194/tc-6-909-2012.

Bottrell, S.H. and Tranter, M. (2002) "Sulphide oxidation under partially anoxic conditions at the bed of the Haut Glacier d'Arolla, Switzerland," Hydrological Processes, 16(12), pp. 2363–2368. Available at: https://doi.org/10.1002/hyp.1012.

Boudreau, B.P. (1997) Diagenetic models and their implementation: Modelling transport and reactions in aquatic sediments. Berlin ; New York: Springer.

Boudreau, B.P. and Ruddick, B.R. (1991) "On a reactive continuum representation of organic matter diagenesis," American Journal of Science, 291(5), pp. 507–538. Available at: https://doi.org/10.2475/ajs.291.5.507.

Bougamont, M., Tulaczyk, S. and Joughin, I. (2003) "Response of subglacial sediments to basal freeze-on 2. Application in numerical modeling of the recent stoppage of Ice Stream C, West Antarctica," Journal of Geophysical Research: Solid Earth, 108(B4), p. 2002JB001936. Available at: https://doi.org/10.1029/2002JB001936.

Boyd, E.S. et al. (2010) "Methanogenesis in subglacial sediments: Subglacial methanogenesis," Environmental Microbiology Reports, 2(5), pp. 685–692. Available at: https://doi.org/10.1111/j.1758-2229.2010.00162.x.

Buchardt, S.L. and Dahl-Jensen, D. (2007) "Estimating the basal melt rate at NorthGRIP using a Monte Carlo technique," Annals of Glaciology, 45, pp. 137–142. Available at: https://doi.org/10.3189/172756407782282435.

Burdige, D.J. et al. (2016) "Methane dynamics in Santa Barbara Basin (USA) sediments as examined with a reaction-transport model," Journal of Marine Research, 74(6), pp. 277–313. Available at: https://doi.org/10.1357/002224016821744151.

Chandler, D.M. et al. (2013) "Evolution of the subglacial drainage system beneath the Greenland Ice Sheet revealed by tracers," Nature Geoscience, 6(3), pp. 195–198. Available at: https://doi.org/10.1038/ngeo1737.

Christ, A.J. et al. (2021) "A multimillion-year-old record of Greenland vegetation and glacial history preserved in sediment beneath 1.4 km of ice at Camp Century," Proceedings of the National Academy of Sciences, 118(13), p. e2021442118. Available at: https://doi.org/10.1073/pnas.2021442118.

Christiansen, J.R. et al. (2021) "Carbon Emissions From the Edge of the Greenland Ice Sheet Reveal Subglacial Processes of Methane and Carbon Dioxide Turnover," Journal of Geophysical Research: Biogeosciences, 126(11). Available at: https://doi.org/10.1029/2021JG006308.

Christiansen, J.R. and Jørgensen, C.J. (2018) "First observation of direct methane emission to the atmosphere from the subglacial domain of the Greenland Ice Sheet," Scientific Reports, 8(1), p. 16623. Available at: https://doi.org/10.1038/s41598-018-35054-7.

Colgan, W. et al. (2022) "Greenland Geothermal Heat Flow Database and Map (Version 1)," Earth System Science Data, 14(5), pp. 2209–2238. Available at: https://doi.org/10.5194/essd-14-2209-2022.

Cowton, T. et al. (2012) "Rapid erosion beneath the Greenland ice sheet," Geology, 40(4), pp. 343–346. Available at: https://doi.org/10.1130/G32687.1.

https://doi.org/10.5194/egusphere-2025-5506
Preprint. Discussion started: 23 December 2025

Dahl-Jensen, D. et al. (2003) “Basal melt at NorthGRIP modeled from borehole, ice-core and radio-echo sounder observations,” Annals of Glaciology, 37, pp. 207–212. Available at: https://doi.org/10.3189/172756403781815492.

Dale, A.W. et al. (2008) “Anaerobic oxidation of methane (AOM) in marine sediments from the Skagerrak (Denmark): II. Reaction-transport modeling,” Geochimica et Cosmochimica Acta, 72(12), pp. 2880–2894. Available at: https://doi.org/10.1016/j.gca.2007.11.039.

Dale, A.W., Regnier, P. and Van Cappellen, P. (2006) “Bioenergetic Controls on Anaerobic Oxidation of Methane (AOM) in Coastal Marine Sediments: A Theoretical Analysis,” American Journal of Science, 306(4), pp. 246–294. Available at: https://doi.org/10.2475/ajs.306.4.246.

De Jong, A.E.E. et al. (2018) “Increases in temperature and nutrient availability positively affect methane-cycling microorganisms in Arctic thermokarst lake sediments,” Environmental Microbiology, 20(12), pp. 4314–4327. Available at: https://doi.org/10.1111/1462-2920.14345.

Dieser, M. et al. (2014) “Molecular and biogeochemical evidence for methane cycling beneath the western margin of the Greenland Ice Sheet,” The ISME Journal, 8(11), pp. 2305–2316. Available at: https://doi.org/10.1038/ismej.2014.59.

Dow, C.F. et al. (2013) “Seismic evidence of mechanically weak sediments underlying Russell Glacier, West Greenland,” Annals of Glaciology, 54(64), pp. 135–141. Available at: https://doi.org/10.3189/2013AoG64A032.

Egger, M. et al. (2018) “Global diffusive fluxes of methane in marine sediments,” Nature Geoscience, 11(6), pp. 421–425. Available at: https://doi.org/10.1038/s41561-018-0122-8.

Graly, J.A. et al. (2014) “Chemical weathering under the Greenland Ice Sheet,” Geology, 42(6), pp. 551–554. Available at: https://doi.org/10.1130/G35370.1.

Graly, J.A., Drever, J.I. and Humphrey, N.F. (2017) “Calculating the balance between atmospheric CO_2 drawdown and organic carbon oxidation in subglacial hydrochemical systems,” Global Biogeochemical Cycles, 31(4), pp. 709–727. Available at: https://doi.org/10.1002/2016GB005425.

Harper, J. et al. (2021) “Generation and fate of basal meltwater during winter, western Greenland Ice Sheet,” The Cryosphere, 15(12), pp. 5409–5421. Available at: https://doi.org/10.5194/tc-15-5409-2021.

Harper, J.T. et al. (2017) “Borehole measurements indicate hard bed conditions, Kangerlussuaq sector, western Greenland Ice Sheet,” Journal of Geophysical Research: Earth Surface, 122(9), pp. 1605–1618. Available at: https://doi.org/10.1002/2017JF004201.

Harrington, J.A., Humphrey, N.F. and Harper, J.T. (2015) “Temperature distribution and thermal anomalies along a flowline of the Greenland ice sheet,” Annals of Glaciology, 56(70), pp. 98–104. Available at: https://doi.org/10.3189/2015AoG70A945.

Hatton, J. et al. (in review) “Pervasive Holocene organics recycled and expelled as methane from beneath the Greenland Ice Sheet,” Nature Geoscience [Preprint].

Hawkings, J.R. et al. (2014) “Ice sheets as a significant source of highly reactive nanoparticulate iron to the oceans,” Nature Communications, 5(1), p. 3929. Available at: https://doi.org/10.1038/ncomms4929.

https://doi.org/10.5194/egusphere-2025-5506
Preprint. Discussion started: 23 December 2025

Hawkings, J.R. et al. (2018) “Biolabile ferrous iron bearing nanoparticles in glacial sediments,” Earth and Planetary Science Letters, 493, pp. 92–101. Available at: https://doi.org/10.1016/j.epsl.2018.04.022.

Hawkings, J.R. et al. (2021) “Large subglacial source of mercury from the southwestern margin of the Greenland Ice Sheet,” Nature Geoscience, 14(7), pp. 496–502. Available at: https://doi.org/10.1038/s41561-021-00753-w.

Herron, S., Hoar and Langway, C.C. (1979) “The Debris-Laden Ice at the Bottom of the Greenland Ice Sheet,” Journal of Glaciology, 23(89), pp. 193–207. Available at: https://doi.org/10.3189/S002214300002983X.

Knoblauch, C. et al. (2008) “Methane turnover and temperature response of methane-oxidizing bacteria in permafrost-affected soils of northeast Siberia,” Soil Biology and Biochemistry, 40(12), pp. 3004–3013. Available at: https://doi.org/10.1016/j.soilbio.2008.08.020.

Kohler, T.J. et al. (2017) “Carbon dating reveals a seasonal progression in the source of particulate organic carbon exported from the Greenland Ice Sheet,” Geophysical Research Letters, 44(12), pp. 6209–6217. Available at: https://doi.org/10.1002/2017GL073219.

Kotsyurbenko, O.R. et al. (2004) “Acetoclastic and hydrogenotrophic methane production and methanogenic populations in an acidic West-Siberian peat bog,” Environmental Microbiology, 6(11), pp. 1159–1173. Available at: https://doi.org/10.1111/j.1462-2920.2004.00634.x.

Kulessa, B. et al. (2017) “Seismic evidence for complex sedimentary control of Greenland Ice Sheet flow,” Science Advances, 3(8), p. e1603071. Available at: https://doi.org/10.1126/sciadv.1603071.

Kulessa, B., Hubbard, B. and Brown, G.H. (2006) “Time-lapse imaging of subglacial drainage conditions using three-dimensional inversion of borehole electrical resistivity data,” Journal of Glaciology, 52(176), pp. 49–57. Available at: https://doi.org/10.3189/172756506781828854.

Lamarche-Gagnon, G. et al. (2019) “Greenland melt drives continuous export of methane from the ice-sheet bed,” Nature, 565(7737), pp. 73–77. Available at: https://doi.org/10.1038/s41586-018-0800-0.

Lawson, E.C. (2012) Investigating Carbon Sourcing and Cycling in Subglacial Environments. Available at: https://doi.org/10.13140/2.1.2359.8406.

Lenstra, W.K. et al. (2023) “Gene-Based Modeling of Methane Oxidation in Coastal Sediments: Constraints on the Efficiency of the Microbial Methane Filter,” Environmental Science & Technology, 57(34), pp. 12722–12731. Available at: https://doi.org/10.1021/acs.est.3c02023.

Maier, N. et al. (2021) “Basal traction mainly dictated by hard-bed physics over grounded regions of Greenland,” The Cryosphere, 15(3), pp. 1435–1451. Available at: https://doi.org/10.5194/tc-15-1435-2021.

Mankoff, K.D. et al. (2020) “Greenland liquid water discharge from 1958 through 2019,” Earth System Science Data, 12(4), pp. 2811–2841. Available at: https://doi.org/10.5194/essd-12-2811-2020.

Mao, S.-H. et al. (2022) “Aerobic oxidation of methane significantly reduces global diffusive methane emissions from shallow marine waters,” Nature Communications, 13(1), p. 7309. Available at: https://doi.org/10.1038/s41467-022-35082-y.

https://doi.org/10.5194/egusphere-2025-5506
Preprint. Discussion started: 23 December 2025

Martinez-Cruz, K. et al. (2017) "Anaerobic oxidation of methane by aerobic methanotrophs in sub-Arctic lake sediments," Science of The Total Environment, 607–608, pp. 23–31. Available at: https://doi.org/10.1016/j.scitotenv.2017.06.187.

Michaud, A.B. et al. (2017) "Microbial oxidation as a methane sink beneath the West Antarctic Ice Sheet," Nature Geoscience, 10(8), pp. 582–586. Available at: https://doi.org/10.1038/ngeo2992.

Morris, M.D. (1991) "Factorial Sampling Plans for Preliminary Computational Experiments," Technometrics, 33(2), pp. 161–174. Available at: https://doi.org/10.1080/00401706.1991.10484804.

Murguia-Flores, F. et al. (2018) "Soil Methanotrophy Model (MeMo v1.0): A process-based model to quantify global uptake of atmospheric methane by soil," Geoscientific Model Development, 11(6), pp. 2009–2032. Available at: https://doi.org/10.5194/gmd-11-2009-2018.

Nilsson, M. and Öuist, M. (2013) "Partitioning Litter Mass Loss into Carbon Dioxide and Methane in Peatland Ecosystems," in A.J. Baird et al. (eds.) Geophysical Monograph Series. Washington, D. C.: American Geophysical Union, pp. 131–144. Available at: https://doi.org/10.1029/2008GM000819.

Oh, Y. et al. (2020) "Reduced net methane emissions due to microbial methane oxidation in a warmer Arctic," Nature Climate Change, 10(4), pp. 317–321. Available at: https://doi.org/10.1038/s41558-020-0734-z.

Olid, C. et al. (2022) "Groundwater discharge as a driver of methane emissions from Arctic lakes," Nature Communications, 13(1), p. 3667. Available at: https://doi.org/10.1038/s41467-022-31219-1.

Pain, A.J. et al. (2021) "Heterogeneous CO_2 and CH_4 content of glacial meltwater from the Greenland Ice Sheet and implications for subglacial carbon processes," The Cryosphere, 15(3), pp. 1627–1644. Available at: https://doi.org/10.5194/tc-15-1627-2021.

Palmer, S. et al. (2011) "Seasonal speedup of the Greenland Ice Sheet linked to routing of surface water," Earth and Planetary Science Letters, 302(3–4), pp. 423–428. Available at: https://doi.org/10.1016/j.epsl.2010.12.037.

Pianosi, F. et al. (2016) "Sensitivity analysis of environmental models: A systematic review with practical workflow," Environmental Modelling & Software, 79, pp. 214–232. Available at: https://doi.org/10.1016/j.envsoft.2016.02.008.

Pianosi, F., Sarrazin, F. and Wagener, T. (2015) "A Matlab toolbox for Global Sensitivity Analysis," Environmental Modelling & Software, 70, pp. 80–85. Available at: https://doi.org/10.1016/j.envsoft.2015.04.009.

Puglini, M. et al. (2019) Assessing the potential for non-turbulent methane escape from the East Siberian Arctic Shelf. preprint. Biogeochemistry: Sediment. Available at: https://doi.org/10.5194/bg-2019-264.

Redfield, A.C. (1934) "On the proportions of organic derivatives in sea water and their relation to the composition of plankton," in James Johnstone Memorial Volume. University Press of Liverpool, pp. 176–192.

Regnier, P. et al. (2002) "Modeling complex multi-component reactive-transport systems: Towards a simulation environment based on the concept of a Knowledge Base," Applied Mathematical Modelling, 26(9), pp. 913–927. Available at: https://doi.org/10.1016/S0307-904X(02)00047-1.

Regnier, P. et al. (2011) "Quantitative analysis of anaerobic oxidation of methane (AOM) in marine sediments: A modeling perspective," Earth-Science Reviews, 106(1–2), pp. 105–130. Available at: https://doi.org/10.1016/j.earscirev.2011.01.002.

https://doi.org/10.5194/egusphere-2025-5506
Preprint. Discussion started: 23 December 2025

Regnier, P., Wollast, R. and Steefel, C.I. (1997) “Long-term fluxes of reactive species in macrotidal estuaries: Estimates from a fully transient, multicomponent reaction-transport model,” Marine Chemistry, 58(1–2), pp. 127–145. Available at: https://doi.org/10.1016/S0304-4203(97)00030-3.

Ruskeeniemi, T. et al. (2018) “Subglacial permafrost evidencing re-advance of the Greenland Ice Sheet over frozen ground,” Quaternary Science Reviews, 199, pp. 174–187. Available at: https://doi.org/10.1016/j.quascirev.2018.09.002.

Saltelli, A. et al. (2007) Global Sensitivity Analysis. The Primer. 1st ed. Wiley. Available at: https://doi.org/10.1002/9780470725184.

Sapper, S.E. et al. (2023) “Methane emissions from subglacial meltwater of three alpine glaciers in Yukon, Canada,” Arctic, Antarctic, and Alpine Research, 55(1), p. 2284456. Available at: https://doi.org/10.1080/15230430.2023.2284456.

Soetaert, K., Herman, P.M.J. and Middelburg, J.J. (1996) “Dynamic response of deep-sea sediments to seasonal variations: A model,” Limnology and Oceanography, 41(8), pp. 1651–1668. Available at: https://doi.org/10.4319/lo.1996.41.8.1651.

Statham, P.J., Skidmore, M. and Tranter, M. (2008) “Inputs of glacially derived dissolved and colloidal iron to the coastal ocean and implications for primary productivity,” Global Biogeochemical Cycles, 22(3), p. 2007GB003106. Available at: https://doi.org/10.1029/2007GB003106.

Stibal, M. et al. (2012) “Methanogenic potential of Arctic and Antarctic subglacial environments with contrasting organic carbon sources,” Global Change Biology, 18(11), pp. 3332–3345. Available at: https://doi.org/10.1111/j.1365-2486.2012.02763.x.

Strock, K.E. et al. (2024) “Oxidation is a potentially significant methane sink in land-terminating glacial runoff,” Scientific Reports, 14(1), p. 23389. Available at: https://doi.org/10.1038/s41598-024-73041-3.

Symons, G.E. and Buswell, A.M. (1933) “The Methane Fermentation of Carbohydrates,” Journal of the American Chemical Society, 55(5), pp. 2028–2036. Available at: https://doi.org/10.1021/ja01332a039.

Telling, J. et al. (2015) “Rock comminution as a source of hydrogen for subglacial ecosystems,” Nature Geoscience, 8(11), pp. 851–855. Available at: https://doi.org/10.1038/ngeo2533.

Thullner, M., Dale, A.W. and Regnier, P. (2009) “Global-scale quantification of mineralization pathways in marine sediments: A reaction-transport modeling approach: QUANTIFICATION OF MINERALIZATION PATHWAYS IN MARINE SEDIMENTS,” Geochemistry, Geophysics, Geosystems, 10(10), pp. n/a–n/a. Available at: https://doi.org/10.1029/2009GC002484.

Tranter, M. et al. (2002) “Geochemical weathering at the bed of Haut Glacier d’Arolla, Switzerland?a new model,” Hydrological Processes, 16(5), pp. 959–993. Available at: https://doi.org/10.1002/hyp.309.

Tranter, M., Skidmore, M. and Wadham, J. (2005) “Hydrological controls on microbial communities in subglacial environments,” Hydrological Processes, 19(4), pp. 995–998. Available at: https://doi.org/10.1002/hyp.5854.

Vinšová, P. et al. (2022) “The Biogeochemical Legacy of Arctic Subglacial Sediments Exposed by Glacier Retreat,” Global Biogeochemical Cycles, 36(3). Available at: https://doi.org/10.1029/2021GB007126.

Vrbická, K. et al. (2022) "Catchment characteristics and seasonality control the composition of microbial assemblages exported from three outlet glaciers of the Greenland Ice Sheet," Frontiers in Microbiology, 13, p. 1035197. Available at: https://doi.org/10.3389/fmicb.2022.1035197.

Wadham, J.L. et al. (2008) "Subglacial methanogenesis: A potential climatic amplifier?: METHANE PRODUCTION UNDER ICE," Global Biogeochemical Cycles, 22(2), pp. n/a–n/a. Available at: https://doi.org/10.1029/2007GB002951.

Wadham, J.L. et al. (2012) "Potential methane reservoirs beneath Antarctica," Nature, 488(7413), pp. 633–637. Available at: https://doi.org/10.1038/nature11374.

Wadham, J.L. et al. (2019) "Ice sheets matter for the global carbon cycle," Nature Communications, 10(1), p. 3567. Available at: https://doi.org/10.1038/s41467-019-11394-4.

Walter, F., Chaput, J. and Lüthi, M.P. (2014) "Thick sediments beneath Greenland's ablation zone and their potential role in future ice sheet dynamics," Geology, 42(6), pp. 487–490. Available at: https://doi.org/10.1130/G35492.1.

Wang, Y. and Van Cappellen, P. (1996) "A multicomponent reactive transport model of early diagenesis: Application to redox cycling in coastal marine sediments," Geochimica et Cosmochimica Acta, 60(16), pp. 2993–3014. Available at: https://doi.org/10.1016/0016-7037(96)00140-8.

Weitemeyer, K.A. and Buffett, B.A. (2006) "Accumulation and release of methane from clathrates below the Laurentide and Cordilleran ice sheets," Global and Planetary Change, 53(3), pp. 176–187. Available at: https://doi.org/10.1016/j.gloplacha.2006.03.014.

Willerslev, E. et al. (2007) "Ancient Biomolecules from Deep Ice Cores Reveal a Forested Southern Greenland," Science, 317(5834), pp. 111–114. Available at: https://doi.org/10.1126/science.1141758.

Yde, J.C. et al. (2010) "Basal ice microbiology at the margin of the Greenland ice sheet," Annals of Glaciology, 51(56), pp. 71–79. Available at: https://doi.org/10.3189/172756411795931976.

Znamínko, M. et al. (2023) "Methylotrophic Communities Associated with a Greenland Ice Sheet Methane Release Hotspot," Microbial Ecology, 86(4), pp. 3057–3067. Available at: https://doi.org/10.1007/s00248-023-02302-x.